This is a preprint, the final version is subject to change, of the American Mineralogist (MSA)
Cite as Authors (Year) Title. American Mineralogist, in press.
(DOI will not work until issue is live.) DOI: http://dx.doi.org/10.2138/am-2017-5952CCBY

Accounting for the species-dependence of the 3500 cm^{-1} H_2O_t infrared molar absorptivity coefficient: implications for hydrated volcanic glasses

REVISION 2

[1]Iona M. McIntosh*, [1]Alexander R.L. Nichols[†], [2]Kenichiro Tani, and [3]Edward W. Llewellin

*Corresponding author

[1]Japan Agency for Marine-Earth Science and Technology (JAMSTEC), 2-15 Natsushima-cho, Yokosuka, Kanagawa 237-0061, Japan

[2]Department of Geology and Paleontology, National Museum of Nature and Science, 4-1-1 Amakubo, Tsukuba, Ibaraki 305-0005, Japan

[3]Department of Earth Sciences, Durham University, Durham DH1 3LE, United Kingdom

[†]Now at: Department of Geological Sciences, University of Canterbury, Christchurch 8140, New Zealand

Author email addresses:

Iona M. McIntosh i.m.mcintosh@jamstec.go.jp

Alexander R.L. Nichols alex.nichols@canterbury.ac.nz

Kenichiro Tani kentani@kahaku.go.jp

Edward W. Llewellin ed.llewellin@durham.ac.uk

This is a preprint, the final version is subject to change, of the American Mineralogist (MSA)
Cite as Authors (Year) Title. American Mineralogist, in press.
(DOI will not work until issue is live.) DOI: http://dx.doi.org/10.2138/am-2017-5952CCBY

Abstract

Fourier Transform Infrared (FTIR) spectroscopy can be used to determine the concentration and speciation of dissolved water in silicate glasses if the molar absorptivity coefficients (ε) are known. Samples that are thin and/or water-poor typically require the use of the mid-IR 3500 cm^{-1} total water (H_2O_t) and 1630 cm^{-1} molecular water (H_2O_m) absorbance bands, from which hydroxyl water (OH) must be determined by difference; however, accurate determination of H_2O_t and OH is complicated because ε3500 varies with water speciation, which is not usually known a priori. We derive an equation that uses endmember ε3500 values to find accurate H_2O_t and OH concentrations from the 3500 cm^{-1} absorbance for samples where only the H_2O_m concentration need be known (e.g. from the 1630 cm^{-1} band). We validate this new species-dependent ε3500 method against published datasets and new analyses of glass standards. We use published data to calculate new endmember ε3500 values of $\varepsilon3500_{OH} = 79 \pm 11$ and $\varepsilon3500_{H_2O_m} = 49 \pm 6$ L/mol·cm for Fe-bearing andesite and $\varepsilon3500_{OH} = 76 \pm 12$ and $\varepsilon3500_{H_2O_m} = 62 \pm 7$ L/mol·cm for Fe-free andesite. These supplement existing endmember values for rhyolite and albite compositions. We demonstrate that accounting for the species-dependence of ε3500 is especially important for hydrated samples, which contain excess H_2O_m, and that accurate measurement of OH concentration, in conjunction with published speciation models, enables reconstruction of original pre-hydration water contents. Although previous studies of hydrous silicate glasses have suggested that values of ε decrease with decreasing tetrahedral cation fraction of the glass, this trend is not seen in the four sets of endmember ε3500 values presented here. We expect that future FTIR studies that derive endmember ε3500 values for additional compositions will therefore not only enable the species-dependent ε3500 method to be applied more widely, but will also offer additional insights into the relationship between values of ε and glass composition.

45 **Keywords:** FTIR, water, H_2O speciation, volcanic glass, rhyolite, andesite, hydration,
46 obsidian

47

Introduction

The dissolved water content of a silicate melt affects a range of magmatic processes, since it exerts a strong influence on melt viscosity (e.g. Hess and Dingwell 1996; Giordano et al. 2008), volatile diffusivities (e.g. Baker et al. 2005; Baker and Alletti 2012), and crystallization (e.g. Hammer 2004; Gualda et al. 2012). Accurate measurement of the water content of silicate glasses is therefore crucial to a wide range of volcanological and petrological studies. Additionally, measuring water speciation, i.e. the amount of water present as molecular water (H_2O_m) versus hydroxyl groups (OH), can provide information about the cooling rate and glass transition temperature (T_g) of a sample (e.g. Stolper 1989; Dingwell and Webb 1990; Xu and Zhang 2002), and whether a sample has been affected by hydration during bubble resorption, or crystallization during cooling (e.g. McIntosh et al. 2014; Nichols et al. 2014), or by secondary hydration at low temperature in the time following deposition (e.g. Dixon et al. 1995; Anovitz et al. 2008; Denton et al. 2009; Tuffen et al. 2010). Whereas most commonly used techniques (e.g. hydrogen manometry, thermogravimetric analysis (TGA), secondary ion mass spectrometry (SIMS)) can measure only total water (H_2O_t) contents, Fourier Transform infrared spectroscopy (FTIR) is capable of measuring both total water and water species concentrations.

FTIR analysis of hydrous glasses

During transmission FTIR analysis, some infrared light passing through the sample is absorbed by molecules within the sample, with different species absorbing light at different, characteristic frequencies. The resulting FTIR spectrum thus exhibits absorbance bands at wavelengths (or wavenumbers, cm^{-1}) corresponding to these different absorbing species. There are four main absorbance bands associated with water dissolved in silicate glasses that can be seen in the near- and mid-IR range (Fig. 1), and their assignments are given in Table 1.

The H_2O_m and OH bands at 5200 cm^{-1} and 4500 cm^{-1} have low absorption intensities and are often not detected in glasses that have low water contents or that require thin samples for analysis (e.g. to avoid bubbles or crystals in the beampath). Additionally, these bands can be difficult to measure accurately in intermediate glass compositions where absorptions by Fe cause curvature of the baseline at high wavenumbers (e.g. Stolper 1982; Ohlhorst et al. 2001; Mandeville et al. 2002), or for samples where the absorptions creating the 4500 cm^{-1} band may be complex (Malfait 2009; Le Losq et al. 2015). In many situations therefore the 3500 cm^{-1} band is used to measure the total water (H_2O_t) concentration, and water speciation is obtained by measuring the 1630 cm^{-1} H_2O_m band and then finding OH indirectly by difference (e.g. Wysoczanski and Tani 2006; Yokoyama et al. 2008; Nichols et al. 2009; McIntosh et al. 2014; Giachetti et al. 2015).

The intensity of the absorbance bands is typically measured as the height of the absorbance peak above the baseline, and is termed the absorbance. These absorbance values are then converted into concentrations via the Beer-Lambert law, which relates the attenuation (absorbance) of light passing through a material to the thickness of the material and the concentration of the absorbing species within it, according to:

$$C = \frac{100\, M\, A}{\rho\, l\, \varepsilon}, \tag{1}$$

where C is the concentration of the species of interest ($C_{H_2O_t}$, $C_{H_2O_m}$, or C_{OH}, in wt%), M is the molecular weight (in g/mol; 18.02 for water), A is the absorbance (no units), ρ is the density (in g/L), l is the thickness of the analyzed area (in cm), and ε is the molar absorptivity coefficient for the absorbance band of interest (in L/mol·cm). If the intensity of the absorbance band is measured using the area enclosed by the peak and the baseline rather than the peak height, then this is termed the integrated absorbance (in cm^{-1}) and ε in Eq. 1 is replaced with ε*, the integrated molar absorptivity (in L/mol·cm^2). Since the value of the

peak area is more sensitive to errors in fitting the baseline than the peak height, it is more common to use the absorbance rather than the integrated absorbance. Values of ε (and ε*) are experimentally determined, and, for a given water absorbance band will vary with the anhydrous glass composition, such as from basalt to rhyolite (Silver et al. 1990; Dixon et al. 1995; Ohlhorst et al. 2001; Mandeville et al. 2002; Seaman et al. 2009; Mercier et al. 2010). Establishing the correct value of ε to use for a given species in glass of a given composition is therefore fundamental to the quantitative use of FTIR spectroscopy.

It has previously been noted that, because the 3500 cm^{-1} absorbance band is the net result of absorptions by both H_2O_m and OH species (Table 1), the correct molar absorptivity coefficient for that band – termed ε3500 – will vary with the ratio of the two species (Newman et al. 1986; Okumura et al. 2003). Since the equilibrium proportions of water species vary with temperature and total water concentration (e.g. Stolper, 1982, 1989), and can be altered by disequilibrium processes such as quench resorption (McIntosh et al. 2014), crystallization (e.g. Nichols et al. 2014) and secondary hydration (e.g. Dixon et al. 1995; Anovitz et al. 2008; Tuffen et al. 2010), the 'true' ε3500 value will also vary accordingly, potentially even across the same sample. This accounts for the wide range in ε3500 values reported in the literature, even among glasses of the same composition. For example, rhyolites, which are the most studied composition to date, have reported ε3500 values ranging from 75 to 95 L/mol·cm (Table 2).

Newman et al. (1986) show that end member molar absorptivity coefficients can be calculated for the 3500 cm^{-1} band; these give the theoretical ε3500 value if all water within the glass were present exclusively as H_2O_m ($\varepsilon 3500_{H_2O_m}$), or exclusively as OH ($\varepsilon 3500_{OH}$). They demonstrate that these coefficients can be used to determine an accurate species-dependent ε3500 value, according to:

$$\varepsilon 3500 = X_{\mathrm{OH}}\, \varepsilon 3500_{\mathrm{OH}} + X_{\mathrm{H_2O_m}}\, \varepsilon 3500_{\mathrm{H_2O_m}}, \quad (2)$$

where X_{OH} and $X_{\mathrm{H_2O_m}}$ are the simple mass fractions of water dissolved as OH or H_2O_m, respectively. For their dataset of hydrous rhyolite compositions, Newman et al. (1986) calculate that $\varepsilon 3500_{\mathrm{OH}} = 100 \pm 2$ and $\varepsilon 3500_{\mathrm{H_2O_m}} = 56 \pm 4$ L/mol·cm. However, as the authors point out, this simple relationship for calculating a species-dependent ε3500 value is of limited analytical use since it requires that the speciation of the sample is already known. This requirement has to date limited the practical use of a species-dependent ε3500 value and many researchers have instead necessarily, albeit somewhat arbitrarily, selected a constant value from the literature. Here we build on the work of Newman et al. (1986) and present a new methodology for accounting for the species-dependence of ε3500, without requiring a priori knowledge of the species proportions. This method enables accurate water species concentrations to be determined from the 3500 cm^{-1} and 1630 cm^{-1} absorbance bands. We demonstrate the effectiveness of this technique by applying it to published datasets and to the analyses of glass standards with known water contents, and then discuss its implications for the analysis of hydrated glasses.

Accounting for species-dependence of ε3500

Calculation of OH concentration using endmember ε3500 values

Equation 2 can be rewritten in terms of species concentrations, using the definitions $X_{\mathrm{OH}} = C_{\mathrm{OH}} / C_{\mathrm{H_2O_t}}$ and $X_{\mathrm{H_2O_m}} = C_{\mathrm{H_2O_m}} / C_{\mathrm{H_2O_t}}$, giving

$$\varepsilon 3500 = \frac{C_{\mathrm{OH}}\, \varepsilon 3500_{\mathrm{OH}} + C_{\mathrm{H_2O_m}}\, \varepsilon 3500_{\mathrm{H_2O_m}}}{C_{\mathrm{H_2O_t}}}. \quad (3)$$

Rearranging for $C_{H_2O_t}$, and substituting into the Beer-Lambert law (Eq. 1), we obtain an expression for the concentration of OH

$$C_{OH} = \frac{1}{\varepsilon 3500_{OH}} \left(\frac{100\, M\, \overline{A}_{3500}}{\rho} - \varepsilon 3500_{H_2O_m} C_{H_2O_m} \right), \quad (4)$$

where $\overline{A}_{3500}$ is the measured 3500 cm^{-1} absorbance normalized for sample thickness (i.e. $\overline{A} = A/l$) in units of 1/cm. With this equation it is now possible to calculate directly the OH concentration of a sample if the glass thickness, 3500 cm^{-1} absorbance, H_2O_m concentration (which can be found from either the 5200 cm^{-1} or 1630 cm^{-1} absorbance band in the conventional way via Eq. 1), and the endmember ε3500 values for the glass composition of interest are known. H_2O_t concentration is then simply $C_{H_2O_t} = C_{OH} + C_{H_2O_m}$.

To test the accuracy of this new species-dependent ε3500 method we apply it to the published dataset of Newman et al. (1986) from which they calculated their endmember ε3500 values for rhyolite. Their dataset consists of samples of natural rhyolitic obsidian from tephra deposits, domes and flows taken from a range of locations in the USA. Thickness data and 5200 cm^{-1}, 4500 cm^{-1} and 3500 cm^{-1} absorbances are reported for 28 analyses of 24 different samples, containing 0.27 – 2.64 wt% H_2O_t as measured by manometry. For these samples, we calculate their H_2O_t and OH concentrations in the conventional way (Eq. 1) using the published 5200 cm^{-1} (H_2O_m) and 4500 cm^{-1} (OH) absorbance data together with the ε5200 and ε4500 values for rhyolite derived by Newman et al. in the same study (Table 2). These are then plotted against the H_2O_t and OH concentrations of the same samples calculated from the published 3500 cm^{-1} (H_2O_t) and 1630 cm^{-1} (H_2O_m) absorbances using our new species-dependent method with the values of $\varepsilon 3500_{OH}$ and $\varepsilon 3500_{H_2O_m}$ for rhyolite derived by Newman et al. (Fig. 2). We find that there is excellent agreement between H_2O_t and OH concentrations calculated by the two methods, as demonstrated by the excellent fit to the 1:1

line ($R^2 = 0.993$ for H_2O_t, and $R^2 = 0.971$ for OH). The 'true' (species-dependent) ε3500 values for individual samples then calculated via Eq. 2 range from 73.6 to 97.2 L/mol·cm, compared to the endmember values of $\varepsilon3500_{OH} = 100 \pm 2$ and $\varepsilon3500_{H_2O_m} = 56 \pm 4$ L/mol·cm.

Calculating endmember ε3500 values for different compositions

New endmember ε3500 values can be calculated for different glass compositions following the procedure of Newman et al. (1986), who showed that the absorbances of the 5200 cm^{-1}, 4500 cm^{-1} and 3500 cm^{-1} bands and their molar absorptivity coefficients can be related as:

$$\overline{A}_{3500} = \frac{\varepsilon3500_{H_2O_m}}{\varepsilon5200}\,\overline{A}_{5200} + \frac{\varepsilon3500_{OH}}{\varepsilon4500}\,\overline{A}_{4500}. \quad (5)$$

This has the form $y = m_1 x_1 + m_2 x_2$, thereby enabling the use of multiple linear regression (e.g. using the Linest function in Microsoft Excel) in order to find the values of $\varepsilon3500_{H_2O_m}/\varepsilon5200$ and $\varepsilon3500_{OH}/\varepsilon4500$ from the measured 5200 cm^{-1} and 4500 cm^{-1} absorbances. Values of ε5200 and ε4500 reported in the literature can then be used to find the two unknowns, i.e. the endmember coefficients $\varepsilon3500_{H_2O_m}$ and $\varepsilon3500_{OH}$.

Thus in order to calculate endmember ε3500 values for a given glass composition, it is necessary to have a dataset containing 5200 cm^{-1}, 4500 cm^{-1} and 3500 cm^{-1} absorbance and thickness data for the same piece(s) of glass, for which the ε5200 and ε4500 values are also known. Since the absorbances are normalized to thickness it is possible to measure the weaker 5200 cm^{-1} and 4500 cm^{-1} absorbances on a thicker piece of glass and then subsequently thin it in order to measure the 3500 cm^{-1} absorbance. Additionally, it would also be possible to use the 1630 cm^{-1} H_2O_m absorbance and ε1630 value in place of the 5200 cm^{-1} H_2O_m absorbance and ε5200 value, if necessary.

We demonstrate this procedure by using the published dataset of Mandeville et al. (2002) to calculate new endmember ε3500 values for both their Fe-bearing and Fe-free andesite compositions. Their samples are hydrous glasses that were synthesized at high pressure and temperature from either a mixture of natural basaltic andesite and evolved andesite rock powders from Krakatau, or a mixture of pure oxide powders and carbonates; H_2O_t contents were measured by hydrogen manometry (see original study for further details). In their dataset, glasses with data for all three bands (5200 cm^{-1}, 4500 cm^{-1} and 3500 cm^{-1}) include two Fe-bearing andesite glasses, Run 9 (1030 °C, 200 MPa, 4.32 wt% H_2O_t, 28 analyses) and Run 101 (1100 °C, 50 MPa, 1.67 wt% H_2O_t, 13 analyses), and three Fe-free andesite glasses, Run 58 (1100 °C, 200 MPa, 5.68 wt% H_2O_t, 56 analyses), Run 68 (1100 °C, 150 MPa, 2.15 wt% H_2O_t, 11 analyses) and Run 106 (1050 °C, 65 MPa, 1.31 wt% H_2O_t, 9 analyses). From the normalized absorbances of these glasses we used the Linest function in Microsoft Excel in order to find values of $\varepsilon3500_{H_2O_m} / \varepsilon5200$ and $\varepsilon3500_{OH} / \varepsilon4500$, as per Eq. 5, for each composition, from which the endmember $\varepsilon3500_{OH}$ and $\varepsilon3500_{H_2O_m}$ coefficients were calculated using the values of ε5200 and ε4500 previously derived and published in the original study (Table 2).

For the Fe-bearing andesite glass compositions reported in Mandeville et al., we thus calculate endmember ε3500 values of $\varepsilon3500_{OH} = 79 \pm 11$ and $\varepsilon3500_{H_2O_m} = 49 \pm 6$ L/mol·cm, while for their Fe-free andesite composition we calculate values of $\varepsilon3500_{OH} = 76 \pm 12$ and $\varepsilon3500_{H_2O_m} = 62 \pm 7$ L/mol·cm. Errors were calculated by propagating the standard error on the regression coefficients and the reported error on the ε5200 and ε4500 values used to derive them via Eq. 5. Fig. 3 compares the H_2O_t and OH concentrations calculated from the 5200 cm^{-1} and 4500 cm^{-1} bands with those calculated from the 3500 cm^{-1} and 1630 cm^{-1} bands using both the species-dependent ε3500 method (Eq. 4) with the new endmember

ε3500 values (filled symbols) and the conventional method (Eq. 1) with the fixed ε3500 value derived by Mandeville et al. (open symbols). For both compositions, the H_2O_t concentrations calculated using the species-dependent ε3500 method are in slightly better agreement with the H_2O_t concentrations calculated from the 5200 cm^{-1} and 4500 cm^{-1} bands than the data calculated using the fixed ε3500 value (Fig. 3 a, c). Meanwhile, the OH concentrations calculated using the species-dependent ε3500 method are in markedly better agreement with the OH concentrations calculated from the 4500 cm^{-1} band than those calculated from the 3500 cm^{-1} band using the conventional OH-by-difference method. For Fe-bearing andesite the OH-by-difference method gives no correlation with OH concentrations derived directly from the 4500 cm^{-1} band (R^2=0.10), whereas the new method gives a much better fit (R^2=0.80; Fig. 3 b). The OH data for Fe-free andesite are somewhat more scattered with regards to the 1:1 line, with most of the scatter corresponding to one glass (Run 58a), but the new method again is closer to the gradient of the 1:1 line and provides a better correlation than the OH-by-difference method, with R^2 values of 0.66 and 0.55 respectively (Fig. 3 d).

A previous study by Silver and Stolper (1989) of H_2O in albitic glasses also followed the method of Newman et al. (1986) in determining endmember ε3500 values for the 3500cm^{-1} band, but since they were similar they elected to publish a single fixed ε3500 value instead. For completeness, we use the published Silver and Stolper dataset (absorbance data for 5 glasses, synthesized at 1500 – 2000 MPa and 1400 – 1600 °C with 1.02 – 5.12 wt% H_2O_t) to calculate that the endmember ε3500 values would be $\varepsilon3500_{OH} = 69 \pm 17$ and $\varepsilon3500_{H_2O_m} = 71 \pm 17$ L/mol·cm, compared to the published fixed ε3500 value of 70 ± 2 L/mol·cm (Table 2).

Application to hydrous glass standards

To further test the accuracy of Eq. 4 we performed transmission FTIR analyses of three glass standards with independently constrained water contents (NWC, KRA-045-2, Run 10).

Chemical compositions and densities of these glasses are reported in Table 3. NWC is a rhyolitic obsidian from the Upper Dome of NW Coulee at Mono Craters, California. A piece of this glass was included in the dataset of Hauri et al. (2002) ("NW Coulee"), whose manometry analysis found it to contain 0.297 wt% H_2O_t. KRA-045-2 is a rhyodacitic obsidian matrix glass from the pyroclastic flow deposit of the 1883 Krakatau eruption (Mandeville et al. 1998), which was analyzed by manometry and found to contain 0.48 wt% H_2O_t (C. Mandeville, published in Maria and Luhr (2008)). Finally, Run 10 is an experimentally synthesized Fe-bearing andesite glass that was part of the dataset of Mandeville et al. (2002), whose manometry analysis gives its total water content as 5.78 wt% H_2O_t.

Methods. All three glasses were prepared for transmission FTIR analysis as double-polished free-standing wafers. The glass thicknesses of the rhyolite standards (NWC and KRA-045-2) were measured using a digital micrometer with a precision of ± 1 μm, with measurements taken at the location of each analysis. Run 10 was too thin, hence fragile, to measure with the micrometer and so thickness was instead calculated from fringes in reflectance spectra following the method of Wysoczanski and Tani (2006) and utilizing a refractive index of 1.55 for andesite (Wohletz and Heiken 1992), with an estimated accuracy of ± 3 μm. FTIR spot analyses were performed at the Japan Agency for Marine-Earth Science and Technology, using a Varian FTS 7000 spectrometer and an attached UMA600 microscope. Mid-IR (6000-700 cm^{-1}) transmittance spectra were collected over 512 scans at a resolution of 8 cm^{-1} using a heated ceramic IR source, a KBr beamsplitter and a liquid nitrogen-cooled $HgCdTe_2$ (MCT) detector. Apertures were used to reduce the beam spot size to 20 x 20 μm. Both the spectrometer bench and microscope were continuously purged with N_2 gas in order to minimize any interference from atmospheric H_2O. Obtained spectra were then processed using Win-IR Pro software. Band absorbances were determined by measuring the height of

the peak above the baseline. For the 3500 cm^{-1} band a linear baseline was used, while for the 4500 cm^{-1} and 1630 cm^{-1} bands baselines were drawn by hand using a flexicurve. H_2O_m concentration was calculated from the 1630 cm^{-1} absorbance via the Beer-Lambert law (Eq. 1) using ε1630 values of 55 ± 2 L/mol·cm for rhyolite (Newman et al. 1986) and 42.34 ± 2.77 L/mol·cm for Fe-bearing andesite (Mandeville et al. 2002). OH concentration was then calculated according to Eq. 4, utilizing the endmember ε3500 values of Newman et al. (1986) for rhyolite and the newly-derived endmember ε3500 values for Fe-bearing andesite. H_2O_t was then calculated as $C_{H_2O_t} = C_{OH} + C_{H_2O_m}$. For comparison, $C_{H_2O_t}$ and C_{OH} (using OH-by-difference) were also calculated from the 3500 cm^{-1} band via Eq. 1 using the range of published fixed ε3500 values (Table 2). For NWC and KRA-045-2 OH concentration was also calculated via Eq. 1 from the 4500 cm^{-1} band using appropriate values of ε4500 (Table 2).

Results. Table 4 and Figs. 4 and 5 show the results of the FTIR spot analyses of the two rhyolite standards, NWC and KRA-045-2, and the Fe-bearing andesite Run 10. Reported values for each sample are the mean value of 12 measurements made on the same wafer. Errors for the rhyolite standards are given as one standard deviation, and for the Fe-bearing andesite are derived from the ± 3 μm error on the thickness measurement, which becomes the dominant source of error for thin samples. For each glass, the H_2O_t concentration measured by FTIR using both the species-dependent ε3500 method and the conventional fixed ε3500 method is plotted against their known H_2O_t content previously measured by manometry (Fig. 4 a, 5 a). For all compositions, the species-dependent ε3500 method (filled squares) gives H_2O_t concentrations that are within 5% of the known value, whereas those calculated using fixed ε3500 values from the literature (open squares) span a wide range and differ from the known H_2O_t concentration by as much as 33%.

OH concentrations calculated using the species-dependent ε3500 method and the conventional OH-by-difference method are compared to the OH concentration obtained from the 4500 cm^{-1} band (Fig. 4 b, Fig. 5 b). For each glass, H_2O_t concentrations determined by summing the 4500 cm^{-1} OH and 1630 cm^{-1} H_2O_m concentrations were compared to their manometry H_2O_t concentration (Fig. 4 c), with the fit to the 1:1 line used to select the most appropriate ε4500 value from the literature (Table 2). Since the weak 4500 cm^{-1} band could not be measured in our thin Run 10 standard we use instead the 4500 cm^{-1} absorbance data reported by Mandeville et al. (2002) for the same glass, and the ε4500 value derived in the same study (Table 2). For the rhyolite standards (Fig. 4 b) the OH concentrations calculated by the species-dependent ε3500 method (filled circles) are within 12% of the 4500 cm^{-1} OH concentration for NWC and within 2% for KRA-045-2, whereas the OH-by-difference concentrations using fixed ε3500 values (open circles) differ by up to 45% and 27% respectively. For the Fe-bearing andesite Run 10 (Fig. 5 b), the species-dependent ε3500 method gives an OH concentration within 9% of that reported by Mandeville et al. (2002). Finding OH-by-difference using the fixed ε3500 value derived by Mandeville et al. (2002) (for the dataset that contained Run 10) matches the 4500 cm^{-1} value exactly, whereas the OH-by-difference derived using the King et al. (2002) fixed ε3500 coefficient is 39% lower than the 4500 cm^{-1} value.

Discussion

Accuracy of H_2O_t and OH concentrations from species-dependent ε3500 method

The new species-dependent ε3500 method is able to reproduce accurately the H_2O_t and OH concentrations of both the published rhyolite and andesite datasets (Figs. 2 and 3) and the hydrous glass standards (Figs. 4 and 5, Table 4). For the datasets, the H_2O_t and OH

300 concentrations derived from the 5200 cm^{-1} H_2O_m and 4500 cm^{-1} OH absorbance bands are not
301 strictly independent measurements since they need ε5200 and ε4500 values to find
302 concentration via the Beer-Lambert law. However, by using the ε5200 and ε4500 values
303 derived from these same datasets in the original studies of Newman et al. (1986) and
304 Mandeville et al. (2002) the resulting concentrations are particularly reliable. The H_2O_t and
305 OH concentrations from the new species-dependent ε3500 method have an excellent
306 correlation with the values derived from the 5200 cm^{-1} and 4500 cm^{-1} bands, demonstrating
307 the accuracy of this technique (Fig. 2 and 3). For the andesite datasets, the species-dependent
308 ε3500 method gives a better fit than the conventional method using fixed ε3500 values.
309 Although the improvement for H_2O_t is only slight, it is particularly marked for OH, where the
310 species-dependent ε3500 method gives much better agreement with the 4500 cm^{-1} OH
311 concentrations than the conventional OH-by-difference method. In particular, the OH-by-
312 difference values for Fe-bearing andesite (Fig. 3 b) give no meaningful correlation to the
313 4500 cm^{-1} OH concentrations ($R^2 = 0.10$) while the species-dependent method gives a much
314 stronger correlation ($R^2 = 0.79$). We therefore strongly recommend the use of the species-
315 dependent ε3500 method for finding the OH concentration when it is necessary to use the
316 3500 absorbance band to do so.

317 Similarly, FTIR analysis of the three glass standards using the species-dependent ε3500
318 method produces H_2O_t and OH concentrations that are within 11% of their independently
319 determined concentrations. The absolute difference is greatest for the Fe-bearing andesite
320 Run 10, where the species-dependent ε3500 method overestimates H_2O_t by 0.11 wt% (Fig. 5
321 a). This discrepancy is most likely due to the need to analyze a thin glass wafer (to avoid
322 saturation of the 3500 cm^{-1} band in this water-rich sample), which increases the relative error
323 owing to the thickness measurement and also creates interference fringes which introduce
324 uncertainty when picking the baseline. Since Run 10 is water-rich however, this error is less

than 2% of the total H_2O_t concentration measured by manometry. By contrast, the H_2O_t concentration calculated for the rhyolite NWC (Fig. 4 a) is only 0.015 wt% higher than the manometry value, but due to the low H_2O_t content of this sample the relative difference is higher (5%). Possible sources of error include slight heterogeneity in water content between the chip that was analyzed with manometry and the chip that was analyzed with FTIR, and differences in how the baseline was picked for the 1630 cm^{-1} H_2O_m peak (see below). Despite these minor discrepancies, the H_2O_t and OH concentrations calculated using the species-dependent ε3500 method are markedly closer to the independently determined concentrations than some of the concentrations calculated using fixed ε3500 values from the literature, which may differ by up to 45% of the known values. Since using a fixed ε3500 value necessarily implies that OH concentration must be found as OH-by-difference, the resulting errors in H_2O_t concentration are also propagated through as errors in OH concentration.

Accuracy of H_2O_m measurement

Since the H_2O_m concentration is needed in order to calculate the species-dependent ε3500 value, any error in the H_2O_m concentration affects the calculated OH and H_2O_t concentrations. When using the 3500 cm^{-1} band, the H_2O_m concentration will generally be determined from the 1630 cm^{-1} band. The ε1630 value for rhyolite comes from Newman et al. (1986) (Table 2), who used the spectrum of an anhydrous equivalent of the glass to define the baseline when measuring 1630 cm^{-1} absorbances, in recognition of the silicate peak at ~1600 cm^{-1} that can interfere with the 1630 cm^{-1} H_2O_m peak and may cause the 1630 cm^{-1} absorbance to be overestimated if using a linear baseline. In lieu of an anhydrous piece of the same glass, we used a hand-drawn flexicurve baseline pinned to the baseline immediately adjacent to the 1630 cm^{-1} peak to account for non-linearity of the baseline. This flexicurve baseline gives an H_2O_m concentration of 0.04 wt% (and subsequent H_2O_t concentration of 0.31 wt%), compared to 0.06 wt% H_2O_m (and 0.32 wt% H_2O_t) if a linear baseline is used. The good

agreement of our flexicurve H_2O_m concentration measurement with the H_2O_m concentrations measured by Newman et al. (1986) for NWC (0.05 wt% using 1630 cm^{-1} band and 0.03 wt% using 5200 cm^{-1} band) validate our method of fitting the 1630 cm^{-1} baseline, and the small difference between our FTIR H_2O_t concentration value and the manometry value (0.015 wt%) indicates that its impact is limited. The weak intensity of the ~1600 cm^{-1} silicate peak means that significant absorbance is restricted to thick sample wafers, while the relative importance of its interference with the 1630 peak is greatest for samples with low H_2O_m concentrations (McIntosh et al. 2015). The error introduced by the 1630 cm^{-1} baseline will therefore be greatest for water-poor samples, but since these samples should contain predominantly OH the ultimate error on the calculated OH and H_2O_t concentrations using the species-dependent ε3500 method will be limited.

The accuracy of the H_2O_m measurement will also necessarily rely on the accuracy of the ε1630 value used to obtain it. When using the 3500 cm^{-1} and 1630 cm^{-1} bands along with a fixed ε3500 value to find OH concentration as $OH = H_2O_t - H_2O_m$, the resulting error for the OH concentration may previously have been attributed to an inaccurate value of ε1630, rather than ε3500. We expect that the use of the species-dependent ε3500 method will reduce or remove such apparent discrepancies in H_2O species concentrations, and that the existing literature values for ε1630 in the compositions discussed in this paper will prove to be robust. It is worth noting that there is evidence that the ε values of the 5200 cm^{-1} and 4500 cm^{-1} bands can vary with H_2O_t concentration (Zhang et al. 1997b; Yamashita et al. 2008). The excellent fit of the H_2O_t and OH concentrations calculated using the species-dependent ε3500 method to the published Newman rhyolite and Mandeville andesite datasets, which span a wide range of H_2O_t concentrations, supports our assumption that the $\varepsilon 3500_{H_2O_m}$ and $\varepsilon 3500_{OH}$ values are true endmember values and do not themselves vary with H_2O_t concentration. It is possible however that in the future a similar H_2O_t-dependence will be found for ε1630 in

some compositions, in which case we expect that our species-dependent ε3500 method can be adapted to account for it. As an example, we show that the H_2O_t-dependent relationship derived for the 5200 cm^{-1} band by Zhang et al. (1997) can be successfully substituted into our method in place of the 1630 cm^{-1} band (see SI spreadsheet). In cases where both the 5200 cm^{-1} and 1630 cm^{-1} bands can be measured for the same glass, we recommend using H_2O_m concentrations calculated from both as input into Eq. 4 in order to check and quantify possible error stemming from the H_2O_m measurement.

Comparison of species-dependent ε3500 and fixed ε3500 values in literature

Since the true ε3500 value is species-dependent, the range in ε3500 values published in the literature results from the differences in the overall speciation (i.e. the ratio of OH to H_2O_m) of the samples used in the different calibration studies. In silicate melts and glasses, the two species interconvert according to the equilibrium reaction:

$$H_2O_{m\,(melt)} + O^{o}_{(melt)} \leftrightarrow 2OH_{(melt)}, \quad (6)$$

in which H_2O_m reacts with bridging oxygens (O^o) to produce OH groups that are bound to the silicate framework (Stolper 1982). For a given melt composition, the position of this equilibrium reaction (i.e. 'equilibrium speciation') is controlled by the temperature and H_2O_t content (e.g. Stolper 1982; Stolper 1989; Nowak and Behrens 1995; Behrens and Nowak 2003; Behrens and Yamashita 2008), with the equilibrium shifted towards OH at high temperature and low H_2O_t, and towards H_2O_m at low temperature and high H_2O_t (Fig. 6). Thus the true value of ε3500 will shift towards the higher $\varepsilon 3500_{OH}$ endmember value for high temperatures and/or low H_2O_t concentrations, and towards the lower $\varepsilon 3500_{H_2O_m}$ endmember value for lower temperatures and/or high H_2O_t concentrations. A final consideration is that the species interconversion reaction rate is strongly temperature dependent and slows dramatically during cooling (Zhang et al. 1991, 1995), until

interconversion becomes negligible and speciation becomes 'frozen in'. The temperature at which this occurs is termed the temperature of apparent equilibrium, T_{ae}, and for a given H_2O_t content will be higher for a fast quench rate (since less time is available at every temperature interval for the reaction to approach equilibrium), and lower for a slow quench rate (e.g. Zhang et al. 1995; Xu and Zhang 2002). T_{ae} has been shown to be equivalent to the temperature of the glass transition, T_g (Dingwell and Webb 1990; Zhang et al. 1997a). However, since T_g is most strictly defined as the glass transition temperature for a melt under a particular set of experimental conditions (e.g. a cooling rate of ~10 K/min), for clarity we use T_{ae} in the following discussion of samples with varied cooling histories. Thus the speciation of rapidly quenched samples will reflect their high T_{ae} by having higher $C_{OH} : C_{H_2O_m}$ ratios, hence higher ε3500 values, than equivalent samples with slower quench and lower T_{ae}.

The variation in published ε3500 values for a given glass composition therefore results from differences in both the water contents and temperature histories of the samples used in each calibration study. For Fe-bearing andesite, Mandeville et al. (2002) derived their fixed ε3500 value of 62.32 ± 0.42 from four glasses synthesized at 1030 – 1130 °C containing 0.21 – 4.32 wt% H_2O_t, with 39 of their 63 analyses stemming from their Run 9 glass (1030 °C, 4.32 wt% H_2O_t), while King et al. (2002) derived a fixed ε3500 value of 70.3 ± 6.86 using glasses synthesized at 1300 °C and containing 0 – 6.09 wt% H_2O_t, of which only 3 out of 43 analyses were made on glasses with >3.39 wt% H_2O_t. The higher ε3500 value of King et al. (2002) therefore likely reflects the lower average H_2O_t content of their samples and their use of a higher experimental temperature and rapid quench rate (with samples quenched to below the glass transition in ~4 s), all of which favor higher $C_{OH} : C_{H_2O_m}$. Applying the fixed ε3500 value of King et al. (2002) to our measurements of the Fe-bearing andesite standard Run 10 underestimates the true H_2O_t content of this glass by 0.72 wt% (Fig. 5 a), highlighting the

potential for large errors when applying a fixed ε3500 value to samples created under different conditions.

Our analyses of the rhyolite standards NWC and KRA-045-2 produced 'true' ε3500 values of 94.7 and 93.1, respectively. These high ε3500 values reflect the dominance of OH at low H_2O_t concentrations (Fig. 6), and are close to the highest fixed ε3500 values reported in the literature: 90 (Hauri et al. 2002), and 95 ± 8 (Aubaud et al. 2009). The calibration of Hauri et al. (2002) was based on a wide range of samples, the majority of which had <0.8 wt% H_2O_t, while that of Aubaud et al. (2009) was based on two samples with <0.16 wt% H_2O_t. At such low H_2O_t contents only negligible H_2O_m would be expected (Fig. 6) and it is therefore reasonable that these fixed ε3500 values should approach the endmember $\varepsilon 3500_{OH}$ value of 100 ± 2 for rhyolite. Although Leschik et al. (2004) found that for glasses with >2 wt% H_2O_t the ε3500 value decreases with increasing H_2O_t concentration (as would be expected due to the increasing proportion of H_2O_m and corresponding shift towards the lower $\varepsilon 3500_{H_2O_m}$ endmember), it is unclear why their fixed ε3500 value of 80 ± 4.9 for water-poor, OH-dominated samples (like our standards) is so much lower than both the Newman et al. $\varepsilon 3500_{OH}$ endmember and other fixed ε3500 values.

By contrast the lowest published value for a fixed ε3500 value for rhyolite (75 ± 4) is that of Okumura et al. (2003), and is based on obsidian samples with 0.24 - 1.25 wt% H_2O_t that were either unheated or heated to 500 – 700°C. The authors noted that ε3500 values derived for the same obsidian source and H_2O_t content (OBSW, 0.74 wt% H_2O_t) increased with the experimental temperature, being 73 for 500°C, 76 for 600°C, and 80 for 700°C. As discussed by the authors, this variation can be explained by the temperature dependence of H_2O speciation that favors higher $C_{OH} : C_{H_2O_m}$, hence higher ε3500, at higher temperatures. Okumura et al. (2003) also derived an ε3500 value for the original unheated obsidian of 77

447 L/mol·cm. Based on their observed temperature dependence of ε3500, we suggest that this
448 value implies that the original T_{ae} of this obsidian was ~620°C. While this indicates that
449 finding the true ε3500 of a sample could be a useful method of finding its T_{ae} ($\approx T_g$), we stress
450 that it is only valid if the temperature dependence of ε3500 is known for samples with exactly
451 the same H_2O_t content. Any derivation of a fixed value of ε3500 is effectively unique to
452 samples with the exact same H_2O_t content and temperature history, hence water speciation, as
453 the samples that were used in its original calibration. Provided that endmember ε3500 values
454 exist for the glass composition of interest, the advantage of our species-dependent ε3500
455 method is that it is possible to obtain accurate H_2O_t and OH concentrations regardless of a
456 sample's H_2O_t content or temperature history, and it can also account for changes in H_2O_t
457 concentration across an individual sample.

458 **Application to hydrated samples**

459 Volcanic glasses are susceptible to secondary hydration, i.e. the addition of water at low
460 temperature in the time following eruption (Friedman and Smith 1958). Hydration of
461 obsidian in particular has a long history of study, not only by the geological, but also the
462 archaeological community, since diffusion modelling of hydration profiles at glass margins
463 could offer a way to date obsidian flows or tools (e.g. Friedman and Long 1976, 1984;
464 Anovitz et al. 1999; Riciputi et al. 2002). Recent studies have also demonstrated that
465 secondary hydration is widespread and has altered the glass water contents of many erupted
466 pyroclasts, with the effect most pronounced for samples with greater surface area exposed to
467 outside water, such as vesicular glasses (e.g. Giachetti and Gonnermann 2013; Dingwell et al.
468 2015). Determining the original eruptive H_2O_t content of hydrated glasses is therefore critical
469 to volatile studies of erupted pyroclasts. Here we use an example of obsidian hydration from
470 the literature to discuss how the species-dependent ε3500 method can be used to measure

accurately the water species concentrations of hydrated glasses, with the potential to thereby reconstruct the original H_2O_t contents of hydrated glasses.

Yokoyama et al. (2008) used transmission FTIR to analyze hydration profiles at the margins of two obsidian flows from Kozushima, Japan, dated to 26,000 and 52,000 years before present. Using the 3500 cm^{-1} and 1630 cm^{-1} bands (and thus finding OH-by-difference), their analyses showed that both H_2O_m and H_2O_t concentrations increase towards the hydrated boundary. The trend in OH concentration was less simple, however, with OH either increasing or decreasing towards the boundary depending on the choice of the fixed ε3500 value. In order to prevent negative OH concentrations, they had to use a fixed ε3500 value of 60; much lower than any of the published values of ε3500 for rhyolite (Table 2). We extracted the concentration data from their published profiles and used their stated values of thickness and density in order to back-calculate their original 3500 cm^{-1} and 1630 cm^{-1} absorbances using the Beer-Lambert law. We then applied our new species-dependent ε3500 method to their absorbances in order to recalculate the H_2O_t and OH concentrations of their hydration profiles, and to calculate the 'true' ε3500 value for every point along the profile (Fig. 7). Doing so, we find that for both profiles the ε3500 value decreases towards the hydrated boundary. Accordingly, the OH concentration profiles no longer exhibit a fall to negative values and remain within 0.1 wt% of their non-hydrated values, while the increase in H_2O_t concentrations towards the boundary becomes more pronounced than in the original profiles.

Since the species interconversion reaction effectively stops at the glass transition temperature (e.g. Dingwell and Webb 1990; Nowak and Behrens 1995; Zhang 1999; Behrens and Nowak 2003; Behrens and Yamashita 2008), water added at ambient temperature during secondary hydration is added as H_2O_m and not interconverted to OH; this creates 'disequilibrium' speciation similar to that which develops during quench resorption (McIntosh et al. 2014).

Glass in the hydrated margin becomes enriched in H_2O_m, and the correct ε3500 value to use will shift towards the $\varepsilon 3500_{H_2O_m}$ endmember value (56 ± 2 for rhyolites). This explains why Yokoyama et al. (2008) had to use an ε3500 value of 60 in order to prevent negative OH concentrations when finding OH-by-difference. This value is much lower than the fixed ε3500 values in the literature, since the literature values were derived from samples with equilibrium rather than H_2O_m-rich disequilibrium speciation. When measuring H_2O_t and OH concentrations of hydrated samples using the 3500 cm^{-1} band, it is therefore imperative that the species-dependence of the ε3500 coefficient is accounted for.

The study of Yokoyama et al. (2008) was limited by the spatial resolution of their FTIR apparatus (they used 15 x 50 μm spots at overlapping 5 μm steps) and we therefore truncate our recalculated profiles at the distance from the edge at which the authors calculated there would be no interference from the adjacent resin. FTIR apparatus with higher spatial resolution, such as those using a synchrotron source (e.g. von Aulock et al. 2014), may be able to investigate the concentration variations in hydrated margins in more detail. Nevertheless, it is clear from the data of Yokoyama et al. (2008) that OH concentration does not increase sharply in the hydration rim whereas the H_2O_m concentration does, supporting their conclusion that the dominant species diffusing into the glass is H_2O_m. A recent study (Bindeman and Lowenstern 2016) on hydration of rhyolite during perlite formation at Yellowstone concluded that hydration occurred at temperatures <200 °C but greater than ambient temperature, over an expected cooling timescale of weeks to years. The authors observed that, although dominated by addition of H_2O_m, this hydration also added minor amounts of OH (~0.2 wt%) to hydrated rims. Our recalculated hydration profile of Yokoyama et al.'s Ohsawa lava (Fig. 7 a) reveals a slight increase in OH concentration from ~0.1 to ~0.2 wt% towards the margin, raising the possibility that its hydration may have occurred under similar conditions to that of the Yellowstone perlite. However, for glasses that

are quenched rapidly to ambient temperature and hydrated subsequently, it is expected that the OH content of a hydrated sample should remain the same as when that sample was first deposited. This is in keeping with observations of volcaniclastic glasses that contain hydrated regions. Those hydrated regions have elevated H_2O_m concentrations, but have similar OH concentrations to unhydrated regions of the same samples (e.g. Nichols et al. 2014). By using the new species-dependent ε3500 method to measure accurately the OH concentration of such hydrated glasses, it is now possible to estimate the original pre-hydration H_2O_t content by using speciation models (e.g. Nowak and Behrens (2001); Fig. 6) to find the H_2O_t concentration that corresponds to the measured OH concentration for the expected T_{ae} ($\approx T_g$) of the sample (e.g. Dingwell et al. 2015). Although the glass transition temperature can vary with cooling history and H_2O_t concentration, OH vs H_2O_t curves for different values of T_g converge at low H_2O_t concentrations (Fig. 6), making this an effective method for glasses with < 1 wt% OH. Other proposed methodologies for reconstructing the original H_2O_t content of hydrated glasses involve thermogravimetric analysis (TGA) (e.g. Denton et al. 2009, 2012; Tuffen et al. 2010; Giachetti et al. 2015) or hydrogen isotope analysis (e.g. DeGroat-Nelson et al. 2001) - both of which produce bulk measurements and destroy the sample - in conjunction with modelling of diffusion, for which some of the parameters are not well constrained for ambient temperatures. This FTIR methodology is relatively cheap and simple to perform, and has the significant benefit of permitting spatial variations in both the original and subsequent H_2O_t concentration to be measured.

Compositional dependence of the molar absorptivity coefficients

It has long been recognized that the values of FTIR molar absorptivity coefficients vary with glass composition (e.g. Silver et al. 1990; Dixon et al. 1995; Ohlhorst et al. 2001; Mandeville et al. 2002; Seaman et al. 2009; Mercier et al. 2010), hence it is unsurprising that the endmember ε3500 values also vary with glass composition. H_2O_t and OH contents derived

546 using the rhyolite endmember coefficients agree well with the manometry data for both of the
547 rhyolite glass standards (Fig. 4), suggesting that these endmember ε3500 values are not
548 sensitive to minor compositional differences, such as a few wt% SiO_2 (Table 3), and can be
549 successfully applied to other glasses with similar major element compositions. However,
550 glasses with greater compositional differences will require their own set of endmember
551 coefficients, as seen in the variation between values for rhyolite, albite, and Fe-bearing and
552 Fe-free andesite (Table 2).

553 Previous studies have suggested that the molar absorptivity coefficients of the H_2O
554 absorption bands decrease with decreasing tetrahedral cation fraction (τ) of the melt, where τ
555 = $(Si^{4+} + Al^{3+})$/total cations (e.g. Dixon et al. 1995; Ohlhorst et al. 2001; Mandeville et al.
556 2002; Seaman et al. 2009; Mercier et al. 2010). Although our data are so far limited to only
557 four glass compositions, our values of $\varepsilon 3500_{OH}$ and $\varepsilon 3500_{H_2O_m}$ do not show a trend with τ
558 (Table 2), and neither do they show a trend with the ratio of non-bridging oxygens over
559 tetrahedrally coordinated cations (NBO/T; Table 2). Although the endmember ε3500 values
560 clearly vary with melt composition, it is not yet possible to simply link this variation with a
561 particular structural parameter that describes the silicate melt.

562 Of the four compositions discussed here, the use of a species-dependent ε3500 is most
563 important for the rhyolite and Fe-andesite compositions. These compositions have the
564 greatest difference between the two endmember coefficients (56–100 and 49–79,
565 respectively) hence the appropriate ε3500 value, and the calculated H_2O_t and OH
566 concentrations, can vary widely. For Fe-free andesite the difference between the endmember
567 coefficients is smaller (62–76) but is still sufficient to justify the use of species-dependent
568 ε3500. On the other hand, the difference between endmember ε3500 values for albite is so
569 small (69–71) that they are within error of each other, which enabled Silver and Stolper

570 (1989) to conclude that there is no advantage in choosing a species-dependent ε3500 value
571 over a fixed ε3500 value for this composition.

572

573 **Implications**

574 Dissolved H_2O content exerts a strong control on silicate melt properties such as viscosity,
575 glass transition temperature, diffusivities of mobile species, and crystallization kinetics.
576 Consequently, for many studies throughout the geological, archeological and materials
577 sciences, it is critical to know accurately the H_2O contents of silicate glasses, even when the
578 behavior of H_2O is not the main focus of the study. The relative ease of sample preparation
579 and low cost of FTIR analyses means that, in many studies of this sort, the H_2O data are
580 obtained by FTIR, and often by analyzing the 3500 cm^{-1} H_2O_t absorbance band. Our new
581 species-dependent ε3500 method, which does not require a change in analytical procedure or
582 expensive instrumentation, will improve the accuracy of these FTIR data, and remove
583 systematic bias in samples that have undergone hydration. Previously published H_2O data
584 that depend upon fixed ε3500 values will therefore need to be re-evaluated to identify and
585 correct potential inaccuracies. This is particularly important given the common use of FTIR
586 H_2O data to constrain glass standards used in the calibration of other analytical techniques
587 such as SIMS (e.g. Hauri et al. 2002). We emphasize that this correction can be accomplished
588 without the need for new instrumental analyses, by simply re-analyzing the raw absorbance,
589 thickness and density data that have already been collected, using the methodology developed
590 in this work. We provide a simple spreadsheet, which accepts these data and performs the
591 relevant calculations, in the supplementary information.

592 The clear advantage of FTIR analysis over other techniques is the ability to obtain
593 quantitative H_2O speciation data, which can be used to investigate topics such as the

mechanisms and rates of H_2O diffusion (e.g. Zhang et al. 1991), or the pressure and temperature histories of glasses (e.g. Zhang et al. 1997a; McIntosh et al. 2014). Many of these studies involve measuring the spatial variation in H_2O species along an H_2O diffusion profile, for example along a diffusion couple experiment or towards a crack, bubble or crystal in the glass (e.g. Zhang et al. 1991; Castro et al. 2008; Berlo et al. 2013; von Aulock et al. 2013; McIntosh et al. 2014; Saubin et al. 2016; Watkins et al. 2016). In such cases, where H_2O_t concentration varies systematically with spatial position, it is essential to account for the species-dependence of ε3500 when using the 3500 cm^{-1} absorbance band, because otherwise errors will also vary systematically with spatial position, as illustrated by our reinterpretation of the Yokoyama et al. hydration profiles (Fig. 7). Removal of this systematic error will significantly improve the quality of interpretations of H_2O speciation data along such profiles.

As well as facilitating reanalysis and reinterpretation of existing studies of experimental and natural hydrous glasses, our new method also opens new avenues of research into glasses affected by secondary hydration. Secondary hydration has been shown to be a widespread phenomenon (e.g. Giachetti and Gonnermann 2013), and we recommend the use of FTIR analyses to identify (by their excess H_2O_m contents) glasses that have been hydrated; information that cannot be obtained by SIMS or Raman spectroscopy. Moreover, improved accuracy of H_2O speciation data along hydration profiles will benefit researchers investigating mechanisms of glass hydration, and the use of obsidian hydration profiles as a dating tool for volcanic and archeological glasses. Most exciting of all, however, is the prospect of estimating the pre-hydration H_2O_t contents of hydrated glasses based on accurate measurement of their OH contents. We propose that this will be a particularly important breakthrough for understanding the eruption processes and associated hazards of silicic submarine eruptions, for which pyroclast glasses are routinely found to be hydrated (e.g. Bryant et al. 2003; Kutterolf et al. 2014). In the same way that the pressure-dependence of

619 H_2O solubility can be used to determine paleo-ice thicknesses from subglacially erupted and
620 quenched glasses (e.g. Tuffen et al. 2010), reconstructed H_2O_t contents of submarine
621 pyroclast glasses can be used to establish the quench depth of unobserved submarine eruption
622 plumes and, in particular, to determine whether pyroclasts now resting on the deep sea floor
623 may have originally reached the sea surface (e.g. Fiske et al. 2001; Tani et al. 2008; Allen et
624 al. 2010; Rotella et al. 2013).

625 Although this paper has focused necessarily on rhyolitic and andesitic glasses, it is hoped that
626 future FTIR studies of hydrous silicate glasses will enable further sets of endmember ε3500
627 values to be derived for more compositions (particularly basalt). This will allow the species-
628 dependent ε3500 method to be applied more widely, and will also improve our understanding
629 of the composition dependence of molar absorptivity coefficients. Such future studies may
630 also improve upon the molar absorptivity coefficients that are available to us today. This
631 study has benefited hugely from the previously published datasets of Newman et al. (1986)
632 and Mandeville et al. (2002), which contained the absorbance, thickness and density data
633 necessary to test and develop our methodology. We therefore strongly advocate for
634 researchers using FTIR data to publish, as we have done here, not only their concentration
635 data but also the absorbance, thickness and density data that underpin them, with the aim of
636 increasing the longevity and relevance of their hard-won data.

637

638 **Acknowledgements**

639 We are grateful to Madeleine Humphreys for providing the glass standards used in this study.
640 We thank Jake Lowenstern and an anonymous reviewer for their thorough and insightful
641 reviews. This research was supported by a Japan Society for the Promotion of Science
642 Postdoctoral Fellowship for Foreign Researchers held by I.M., and a JSPS Grant-in-Aid for

643 Scientific Research (Kakenhi grant number 00470120) awarded to A.R.L.N and I.M.; E.W.L.
644 acknowledges support from the UK Natural Environment Research Council via grant
645 NE/N002954/1.

646

References

Allen, S.R., Fiske, R.S., and Tamura, Y. (2010) Effects of water depth on pumice formation in submarine domes at Sumisu, Izu-Bonin arc, western Pacific. Geology, 38, 391–394.

Anovitz, L.M., Elam, J.M., Riciputi, L.R., and Cole, D.R. (1999) The Failure of Obsidian Hydration Dating: Sources, Implications, and New Directions. Journal of Archaeological Science, 26, 735–752.

Anovitz, L.M., Cole, D.R., and Fayek, M. (2008) Mechanisms of rhyolitic glass hydration below the glass transition. American Mineralogist, 93, 1166–1178.

Aubaud, C., Bureau, H., Raepsaet, C., Khodja, H., Withers, A.C., Hirschmann, M.M., and Bell, D.R. (2009) Calibration of the infrared molar absorption coefficients for H in olivine, clinopyroxene and rhyolitic glass by elastic recoil detection analysis. Chemical Geology, 260, 286–294.

Baker, D.R., and Alletti, M. (2012) Fluid saturation and volatile partitioning between melts and hydrous fluids in crustal magmatic systems: The contribution of experimental measurements and solubility models. Earth-Science Reviews, 114, 298–324.

Baker, D.R., Freda, C., Brooker, R.A., and Scarlato, P. (2005) Volatile diffusion in silicate melts and its effects on melt inclusions. Annals of Geophysics, 48, 699–717.

Behrens, H., and Nowak, M. (2003) Quantification of H2O Speciation in Silicate Glasses and Melts by IR Spectroscopy - in situ versus Quench Techniques. Phase Transitions, 76, 45–61.

Behrens, H., and Yamashita, S. (2008) Water speciation in hydrous sodium tetrasilicate and hexasilicate melts: Constraint from high temperature NIR spectroscopy. Chemical Geology, 256, 305–314.

Berlo, K., Tuffen, H., Smith, V.C., Castro, J.M., Pyle, D.M., Mather, T.A., and Geraki, K. (2013) Element variations in rhyolitic magma resulting from gas transport. Geochimica et Cosmochimica Acta, 121, 436–451.

Bindeman, I.N., and Lowenstern, J.B. (2016) Low-δD hydration rinds in Yellowstone perlites record rapid syneruptive hydration during glacial and interglacial conditions. Contributions to Mineralogy and Petrology, 171, 89.

Bryant, C.J., Arculus, R.J., and Eggins, S.M. (2003) The geochemical evolution of the Izu-Bonin arc system: A perspective from tephras recovered by deep-sea drilling. Geochemistry, Geophysics, Geosystems, 4, 1094.

Castro, J.M., Beck, P., Tuffen, H., Nichols, A.R.L., Dingwell, D.B., and Martin, M.C. (2008) Timescales of spherulite crystallization in obsidian inferred from water concentration profiles. American Mineralogist, 93, 1816–1822.

DeGroat-Nelson, P.J., Cameron, B.I., Fink, J.H., and Holloway, J.R. (2001) Hydrogen isotope analysis of rehydrated silicic lavas : implications for eruption mechanisms. Earth and Planetary Science Letters, 185, 331–341.

Denton, J.S., Tuffen, H., Gilbert, J.S., and Odling, N. (2009) The hydration and alteration of perlite and rhyolite. Journal of the Geological Society, 166, 895–904.

Denton, J.S., Tuffen, H., and Gilbert, J.S. (2012) Variations in hydration within perlitised rhyolitic lavas—evidence from Torfajökull, Iceland. Journal of Volcanology and Geothermal Research, 223–224, 64–73.

Dingwell, D.B., and Webb, S.L. (1990) Relaxation in silicate melts, 2, 427–229.

Dingwell, D.B., Lavallée, Y., Hess, K.-U., Flaws, A., Marti, J., Nichols, A.R.L., Gilg, H.A., and Schillinger, B. (2015) Eruptive shearing of tube pumice: pure and simple. Solid

693 Earth Discussions, 7, 3053–3085.

694 Dixon, J.E., Stolper, E.M., and Holloway, J.R. (1995) An Experimental Study of Water and
695 Carbon Dioxide Solubilities in Mid-Ocean Ridge Basaltic Liquids. Part I: Calibration
696 and Solubility Models. Journal of Petrology, 36, 1607–1631.

697 Dobson, P., Epstein, S., and Stolper, E.M. (1989) Hydrogen isotope fractionation between
698 coexisting vapor and silicate glasses and melts at low pressure. Geochimica et
699 Cosmochimica Acta, 53, 2723–2730.

700 Fiske, R.S., Naka, J., Iizasa, K., Yuasa, M., and Klaus, A. (2001) Submarine silicic caldera at
701 the front of the Izu-Bonin arc, Japan: Voluminous seafloor eruptions of rhyolite pumice.
702 Bulletin of the Geological Society of America, 113, 813–824.

703 Friedman, I., and Long, W. (1976) Rate of Obsidian Hydration. Science, 191, 347–352.

704 ——— (1984) Volcanic glasses, their origins and alteration processes. Journal of Non-
705 Crystalline Solids, 67, 127–133.

706 Friedman, I., and Smith, R.L. (1958) The deuterium content of water in some volcanic
707 glasses. Geochimica et Cosmochimica Acta, 15, 218–228.

708 Giachetti, T., and Gonnermann, H.M. (2013) Water in volcanic pyroclast: Rehydration or
709 incomplete degassing? Earth and Planetary Science Letters, 369–370, 317–332.

710 Giachetti, T., Gonnermann, H.M., Gardner, J.E., Shea, T., and Gouldstone, A. (2015)
711 Discriminating secondary from magmatic water in rhyolitic matrix-glass of volcanic
712 pyroclasts using thermogravimetric analysis. Geochimica et Cosmochimica Acta, 148,
713 457–476.

714 Giordano, D., Russell, J.K., and Dingwell, D.B. (2008) Viscosity of magmatic liquids: A
715 model. Earth and Planetary Science Letters, 271, 123–134.

716 Gualda, G.A.R., Ghiorso, M.S., Lemons, R. V., and Carley, T.L. (2012) Rhyolite-MELTS: a
717 Modified Calibration of MELTS Optimized for Silica-rich, Fluid-bearing Magmatic
718 Systems. Journal of Petrology, 53, 875–890.

719 Hammer, J.E. (2004) Crystal nucleation in hydrous rhyolite: Experimental data applied to
720 classical theory. American Mineralogist, 89, 1673–1679.

721 Hauri, E., Wang, J., Dixon, J.E., King, P.L., Mandeville, C., and Newman, S. (2002) SIMS
722 analysis of volatiles in silicate glasses 1. Calibration, matrix effects and comparisons
723 with FTIR. Chemical Geology, 183, 99–114.

724 Hess, K.-U., and Dingwell, D.B. (1996) Viscosities of hydrous leucogranitic melts : A non-
725 Arrhenian model. American Mineralogist, 81, 1297–1300.

726 Ihinger, P.D., Hervig, R.L., and McMillan, P.F. (1994) Analytical methods for volatiles in
727 glasses. Reviews in Mineralogy and Geochemistry, 30, 67–121.

728 King, P.L., Vennemann, T.W., Holloway, J.R., Hervig, R.L., Lowenstern, J.B., and Forneris,
729 J.F. (2002) Analytical techniques for volatiles: A case study using intermediate
730 (andesitic) glasses. American Mineralogist, 87, 1077–1089.

731 Kutterolf, S., Schindlbeck, J.C., Scudder, R.P., Murray, R.W., Pickering, K.T., Freundt, A.,
732 Labanieh, S., Heydolph, K., Saito, S., Naruse, H., and others (2014) Large volume
733 submarine ignimbrites in the Shikoku Basin: An example for explosive volcanism in the
734 Western Pacific during the Late Miocene. Geochemistry Geophysics Geosystems, 15,
735 1837–1851.

736 Le Losq, C., Cody, G.D., and Mysen, B.O. (2015) Complex IR spectra of OH– groups in
737 silicate glasses: Implications for the use of the 4500 cm–1 IR peak as a marker of OH-
738 groups concentration. American Mineralogist, 100, 945–950.

739 Leschik, M., Heide, G., Frischat, G.H., Behrens, H., Wiedenbeck, M., Wagner, N., Heide, K.,
740 Geissler, H., and Reinholz, U. (2004) Determination of H2O and D2O contents in
741 rhyolitic glasses. Physics and Chemistry of Glasses, 45, 238–251.

742 Malfait, W.J. (2009) The 4500 cm-1 infrared absorption band in hydrous aluminosilicate
743 glasses is a combination band of the fundamental (Si,Al)-OH and O-H vibrations.
744 American Mineralogist, 94, 849–852.

745 Mandeville, C.W., Sasaki, A., Saito, G., Faure, K., King, R., and Hauri, E. (1998) Open-
746 system degassing of sulfur from Krakatau 1883 magma. Earth and Planetary Science
747 Letters, 160, 709–722.

748 Mandeville, C.W., Webster, J.D., Rutherford, M.J., Taylor, B.E., Timbal, A., and Faure, K.
749 (2002) Determination of molar absorptivities for infrared absorption bands of H2O in
750 andesitic glasses. American Mineralogist, 87, 813–821.

751 Maria, A.H., and Luhr, J.F. (2008) Lamprophyres, Basanites, and Basalts of the Western
752 Mexican Volcanic Belt: Volatile Contents and a Vein-Wallrock Melting Relationship.
753 Journal of Petrology, 49, 2123–2156.

754 McIntosh, I.M., Llewellin, E.W., Humphreys, M.C.S., Nichols, A.R.L., Burgisser, A., and
755 Schipper, C.I. (2014) Distribution of dissolved water in magmatic glass records growth
756 and resorption of bubbles. Earth and Planetary Science Letters, 401, 1–11.

757 McIntosh, I.M., Nichols, A.R.L., Schipper, C.I., and Stewart, B. (2015) Glass composition-
758 dependent silicate absorption peaks in FTIR spectroscopy: implications for measuring
759 sample thickness and molecular H2O. In American Geophysical Union Fall Meeting p.
760 V23B–3092.

761 Mercier, M., Di Muro, A., Métrich, N., Giordano, D., Belhadj, O., and Mandeville, C.W.

762 (2010) Spectroscopic analysis (FTIR, Raman) of water in mafic and intermediate glasses
763 and glass inclusions. Geochimica et Cosmochimica Acta, 74, 5641–5656.

764 Newman, S., Stolper, E.M., and Epstein, S. (1986) Measurement of water in rhyolitic glasses:
765 Calibration of an infrared spectroscopic technique. American Mineralogist, 71, 1527–
766 1541.

767 Nichols, A.R.L., Potuzak, M., and Dingwell, D.B. (2009) Cooling rates of basaltic
768 hyaloclastites and pillow lava glasses from the HSDP2 drill core. Geochimica et
769 Cosmochimica Acta, 73, 1052–1066.

770 Nichols, A.R.L., Beier, C., Brandl, P.A., Buchs, D.M., and Krumm, S.H. (2014)
771 Geochemistry of volcanic glasses from the Louisville Seamount Trail (IODP Expedition
772 330): Implications for eruption environments and mantle melting. Geochemistry,
773 Geophysics, Geosystems, 15, 1–21.

774 Nowak, M., and Behrens, H. (1995) The speciation of water in haplogranitic glasses and
775 melts determined by in situ near-infrared spectroscopy. Geochimica et Cosmochimica
776 Acta, 59, 3445–3450.

777 Ohlhorst, S., Behrens, H., and Holtz, F. (2001) Compositional dependence of molar
778 absorptivities of near-infrared OH- and H2O bands in rhyolitic to basaltic glasses.
779 Chemical Geology, 174, 5–20.

780 Okumura, S., and Nakashima, S. (2005) Molar absorptivities of OH and H2O in rhyolitic
781 glass at room temperature and at 400-600 °C. American Mineralogist, 90, 441–447.

782 Okumura, S., Nakamura, M., and Nakashima, S. (2003) Determination of molar absorptivity
783 of IR fundamental OH-stretching vibration in rhyolitic glasses. American Mineralogist,
784 88, 1657–1662.

785 Riciputi, L.R., Elam, J.M., Anovitz, L.M., and Cole, D.R. (2002) Obsidian Diffusion Dating
786 by Secondary Ion Mass Spectrometry: A Test using Results from Mound 65, Chalco,
787 Mexico. Journal of Archaeological Science, 29, 1055–1075.

788 Rotella, M.D., Wilson, C.J.N., Barker, S.J., and Wright, I.C. (2013) Highly vesicular pumice
789 generated by buoyant detachment of magma in subaqueous volcanism. Nature
790 Geoscience, 6, 129–132.

791 Saubin, E., Tuffen, H., Gurioli, L., Owen, J., Castro, J.M., Berlo, K., McGowan, E.M.,
792 Schipper, C.I., and Wehbe, K. (2016) Conduit Dynamics in Transitional Rhyolitic
793 Activity Recorded by Tuffisite Vein Textures from the 2008–2009 Chaitén Eruption.
794 Frontiers in Earth Science, 4, 1–17.

795 Seaman, S.J., Dyar, M.D., and Marinkovic, N. (2009) The effects of heterogeneity in magma
796 water concentration on the development of flow banding and spherulites in rhyolitic lava.
797 Journal of Volcanology and Geothermal Research, 183, 157–169.

798 Silver, L.A., and Stolper, E. (1989) Water in Albitic Glasses. Journal of Petrology, 30, 667–
799 709.

800 Silver, L.A., Ihinger, P.D., and Stolper, E.M. (1990) The influence of bulk composition on
801 the speciation of water in silicate glasses. Contributions to Mineralogy and Petrology,
802 104, 142–162.

803 Stolper, E.M. (1982) The speciation of water in silicate melts. Geochimica et Cosmochimica
804 Acta, 46, 2609–2620.

805 Stolper, E.M. (1982) Water in Silicate Glasses: An Infrared Spectroscopic Study.
806 Contributions to Mineralogy and Petrology, 81, 1–17.

807 Stolper, E.M. (1989) Temperature dependence of the speciation of water in rhyolitic melts

808 and glasses. American Mineralogist, 74, 1247–1257.

809 Tani, K., Fiske, R.S., Tamura, Y., Kido, Y., Naka, J., Shukuno, H., and Takeuchi, R. (2008)
810 Sumisu volcano, Izu-Bonin arc, Japan: Site of a silicic caldera-forming eruption from a
811 small open-ocean island. Bulletin of Volcanology, 70, 547–562.

812 Tuffen, H., Owen, J., and Denton, J. (2010) Magma degassing during subglacial eruptions
813 and its use to reconstruct palaeo-ice thicknesses. Earth-Science Reviews, 99, 1–18.

814 Vetere, F., Behrens, H., Holtz, F., and Neuville, D. (2006) Viscosity of andesitic melts—new
815 experimental data and a revised calculation model. Chemical Geology, 228, 233–245.

816 von Aulock, F.W., Nichols, A.R.L., Kennedy, B.M., and Oze, C. (2013) Timescales of
817 texture development in a cooling lava dome. Geochimica et Cosmochimica Acta, 114,
818 72–80.

819 von Aulock, F.W., Kennedy, B.M., Schipper, C.I., Castro, J.M., E. Martin, D., Oze, C.,
820 Watkins, J.M., Wallace, P.J., Puskar, L., Bégué, F., and others (2014) Advances in
821 Fourier transform infrared spectroscopy of natural glasses: From sample preparation to
822 data analysis. Lithos, 206–207, 52–64.

823 Watkins, J.M., Gardner, J.E., and Befus, K.S. (2017) Nonequilibrium degassing, regassing,
824 and vapor fluxing in magmatic feeder systems. Geology, 45, 183–186.

825 Wohletz, K.H., and Heiken, G. (1992) Volcanology and Geothermal Energy. University of
826 California Press.

827 Wysoczanski, R., and Tani, K. (2006) Spectroscopic FTIR imaging of water species in silicic
828 volcanic glasses and melt inclusions: An example from the Izu-Bonin arc. Journal of
829 Volcanology and Geothermal Research, 156, 302–314.

830 Xu, Z., and Zhang, Y. (2002) Quench rates in air, water, and liquid nitrogen, and inference of

temperature in volcanic eruption columns. Earth and Planetary Science Letters, 200, 315–330.

Yamashita, S., Behrens, H., Schmidt, B.C., and Dupree, R. (2008) Water speciation in sodium silicate glasses based on NIR and NMR spectroscopy. Chemical Geology, 256, 231–241.

Yokoyama, T., Okumura, S., and Nakashima, S. (2008) Hydration of rhyolitic glass during weathering as characterized by IR microspectroscopy. Geochimica et Cosmochimica Acta, 72, 117–125.

Zhang, Y. (1999) H2O IN RHYOLITIC GLASSES AND MELTS: MEASUREMENT, SPECIATION, SOLUBILITY, AND DIFFUSION. Reviews of Geophysics, 37, 493–516.

Zhang, Y., Stolper, E.M., and Wasserburg, G.J. (1991) Diffusion of water in rhyolitic glasses. Geochimica et Cosmochimica Acta, 55, 441–56.

Zhang, Y., Stolper, E.M., and Ihinger, P.D. (1995) Kinetics of the reaction H2O + O = 2OH in rhyolitic and albitic glasses: Preliminary results. American Mineralogist, 80, 593–612.

Zhang, Y., Jenkins, J., and Xu, Z. (1997a) Kinetics of the reaction H2O+O=2OH in rhyolitics glasses upon cooling: Geospeedometry and comparison with glass transition. Geochimica et Cosmochimica Acta, 61, 2167–2173.

Zhang, Y., Belcher, R., Ihinger, P.D., Wang, L., Xu, Z., and Newman, S. (1997b) New calibration of infrared measurement of dissolved water in rhyolitic glasses. Geochimica et Cosmochimica Acta, 61, 3089–3100.

853 **List of figure captions**

854

855 **Figure 1:** H_2O absorbance bands in FTIR spectra of hydrous rhyolite glasses. The 5200 cm^{-1}
856 and 4500 cm^{-1} bands can be seen in the thick, water-rich glass (grey spectrum), but the mid-
857 IR bands are oversaturated. In the thinner, water-poor NWC glass (black spectrum, this
858 study), the 5200 cm^{-1} band is undersaturated and the 4500 cm^{-1} band is only weakly seen, but
859 the 3500 cm^{-1} and 1630 cm^{-1} bands can be seen. A small doublet can be seen at ~2350 cm^{-1}
860 due to molecular CO_2 in the atmosphere. Inset compares choice of linear and flexicurve
861 baselines for 1630 cm^{-1} band.

862

863 **Figure 2:** Validation of the species-dependent ε3500 method for rhyolite. H_2O_t (squares) and
864 OH (circles) concentrations calculated from the 3500 cm^{-1} and 1630 cm^{-1} bands using the
865 species-dependent ε3500 method (i.e. with H_2O_m concentration calculated from the 1630 cm^{-1}
866 band via Eq. 1 and used as an input for Eq. 4 in order to calculate OH concentration, hence
867 H_2O_t concentration) are compared to those derived from the 5200 cm^{-1} and 4500 cm^{-1} bands
868 for the published dataset of Newman et al. (1986). Solid line indicates the 1:1 line. Error bars
869 calculated by propagating uncertainties on all values of ε.

870

871 **Figure 3:** Validation of the species-dependent ε3500 method for andesite. H_2O_t (squares) and
872 OH (circles) concentrations calculated from the 3500 cm^{-1} and 1630 cm^{-1} bands using the
873 species-dependent ε3500 method (filled symbols) are compared to those derived from the
874 5200 cm^{-1} and 4500 cm^{-1} bands for the published dataset of Mandeville et al. (2002) for (**a**, **b**)
875 Fe-bearing andesite and (**c**, **d**) Fe-free andesite. H_2O_t and OH-by-difference concentrations
876 calculated using the fixed ε3500 values of the Mandeville et al. study are shown for
877 comparison (open symbols). Solid line indicates the 1:1 line. For clarity, errors calculated

878 from uncertainties on all values of ε used by each method are shown as symbols with
879 representative error bars on the right-hand margin of each figure tile.
880
881 **Figure 4:** FTIR analyses of rhyolite standards NWC and KRA-045-2. (**a**) H_2O_t
882 concentrations calculated from the 3500 cm^{-1} and 1630 cm^{-1} bands using the species-
883 dependent ε3500 method (filled squares) are compared to the H_2O_t content measured by
884 manometry. Open squares show H_2O_t calculated using the range of fixed ε3500 values for
885 rhyolite in the literature (letters indicate source studies for the different ε3500 values used,
886 see Table 2 for key to labels). (**b**) OH concentrations calculated from the 3500 cm^{-1} and 1630
887 cm^{-1} bands using the species-dependent ε3500 method (filled circles) are compared to the OH
888 concentrations calculated from the measured 4500 cm^{-1} band via the Beer-Lambert law (Eq.
889 1). Open circles show OH-by-difference calculated using the range of fixed ε3500 values for
890 rhyolite in the literature. (**c**) Comparison of H_2O_t concentrations measured by manometry
891 with those calculated from the 5200 cm^{-1} and 4500 cm^{-1} bands using different ε4500 values
892 for rhyolite in the literature (see Table 2 for key to labels). The ε4500 values that give the
893 closest fit to the 1:1 line (filled squares) are the values used to determine OH concentration
894 from the 4500 absorbance for each standard in (**b**). Solid lines indicate 1:1 lines. Error bars
895 represent one standard deviation.
896
897 **Figure 5:** FTIR analysis of Fe-bearing andesite standard Run 10. (**a**) H_2O_t concentrations
898 calculated from the 3500 cm^{-1} and 1630 cm^{-1} bands using the species-dependent ε3500
899 method (filled squares) are compared to the H_2O_t content measured by manometry. Open
900 squares show H_2O_t calculated using the range of fixed ε3500 values for Fe-bearing andesite
901 in the literature (letters indicate source studies for the different ε3500 values used, see Table
902 2 for key to labels). (**b**) OH concentrations calculated from the 3500 cm^{-1} and 1630 cm^{-1}

absorbance bands using the species-dependent ε3500 method (filled circles) are compared to the OH concentrations calculated from the 4500 cm^{-1} band via the Beer-Lambert law (Eq. 1). Since the Run 10 sample was too thin to measure the 4500 cm^{-1} band we use instead the 4500 absorbance reported for this glass in Mandeville et al. (2002). Open circles show OH-by-difference calculated using the range of fixed ε3500 values for Fe-bearing andesite in the literature. Solid lines indicate 1:1 lines. Error bars are derived from the ± 3 μm error on the thickness measurement of this thin sample.

Figure 6: Example of experimentally-determined water speciation model showing variation in OH and H_2O_m concentration with H_2O_t concentration at different temperatures for haplogranite composition (Nowak and Behrens 2001). OH is the dominant species at low H_2O_t concentrations and higher temperatures.

Figure 7: Recalculation of the obsidian hydration profiles published by Yokoyama et al. (2008) for (**a**) Ohsawa and (**b**) Awanomikoto lavas from Kozushima, Japan. The original profiles (open symbols) were obtained using a fixed value of ε3500 = 74 and are shown alongside H_2O_t and OH profiles recalculated using the species-dependent ε3500 method (filled symbols). Note the negative OH values in the original Awanomikoto profile (**b**). The vertical black dashed lines represent the position of the glass edge; profiles are truncated where Yokoyama et al. (2008) calculated that there would be no contamination from the adjacent resin. (**c**, **d**) The 'true' (species-dependent) ε3500 values calculated for each position in the recalculated profiles are shown with reference to the ε3500 endmember values for rhyolite and the original choice of fixed ε3500 = 74.

Deposit items

A Microsoft Excel spreadsheet will be made available online that contains the equations in this paper for using the species-dependent ε3500 method and for deriving new endmember ε3500 values from absorbance data.

Tables

Table 1: Assignments of the major H_2O IR absorbance bands in silicate glasses.

Band	Assignment
5200 cm^{-1}	Combination stretching and bending modes of water molecules
4500 cm^{-1}	Combination stretching and bending modes of structural SiOH and AlOH groups
3500 cm^{-1}	Fundamental OH stretching vibration of both water molecules and structural SiOH and AlOH groups, with the distribution of H-bond strengths between the different species causing the band's breadth and asymmetry
1630 cm^{-1}	Fundamental bending mode of water molecules

This is a preprint, the final version is subject to change, of the American Mineralogist (MSA)
Cite as Authors (Year) Title. American Mineralogist, in press.
(DOI will not work until issue is live.) DOI: http://dx.doi.org/10.2138/am-2017-5952CCBY

936 **Table 2: H_2O molar absorptivity coefficients for rhyolite, Fe-bearing and Fe-free andesite, and albite compositions.**

						Endmember ε3500			
Composition	**τ**	**NBO/T**	**ε5200**	**ε4500**	**Fixed ε3500**	**$\varepsilon3500_{OH}$**	**$\varepsilon3500_{H_2O_m}$**	**ε1630**	**Reference**
Rhyolite	0.859	0.02	1.61 ± 0.05	1.73 ± 0.02		**100 ± 2**	**56 ± 4**	55 ± 2	**N**: 1
					75 ± 4				**O**: 2
			1.86 ± 0.05	1.50 ± 0.10	80 ± 4				**I**: 3
					80 ± 4.9[b]				**L**: 4
					88 ± 2				**D**: 5
					90				**H**: 6
					95 ± 8				**A**: 7
			1.75 ± 0.08	1.42 ± 0.12					**ON**: 8
Fe-bearing andesite	0.746	0.32				**79 ± 11**	**49 ± 6**		**This study[a]**
			1.07 ± 0.07	0.79 ± 0.07	62.32 ± 0.42			42.34 ± 2.77	**M**: 9
			1.08 ± 0.11	1.15 ± 0.17	70.32 ± 6.86			40.83 ± 4.12	**K**: 10
Fe-free andesite	0.795	0.18				**76 ± 12**	**62 ± 7**		**This study[a]**
			1.46 ± 0.07	0.89 ± 0.07	69.21 ± 0.52			52.05 ± 2.85	**M**: 9
			1.04 ± 0.04	0.92 ± 0.03					**V**: 11
Albite	0.800	0.00				**69 ± 17**	**71 ± 17**		**This study[a]**
			1.67 ± 0.06	1.13 ± 0.04	70 ± 2			49 ± 2	12

937

938 Notes: Published coefficients are from [1]Newman et al. (1986), [2]Okumura et al. (2003), [3]Ihinger et al. (1994), [4]Leschik et al. (2004) [5]Dobson et al.
939 (1989), [6]Hauri et al. (2002), [7]Aubaud et al. (2009), [8]Okumura and Nakashima (2005), [9]Mandeville et al. (2002), [10]King et al. (2002), [11]Vetere et
940 al. (2006) and [12]Silver and Stolper (1989). [a]Endmember ε3500 values derived during this study are based on the datasets of [9]Mandeville et al.
941 (2002) (Fe-bearing and Fe-free andesite compositions) and [12]Silver and Stolper (1989) (albite composition). $\tau = (Si^{4+} + Al^{3+})$/total cations, as

942 calculated by [9]Mandeville et al. (2002). NBO/T is the ratio of non-bridging oxygens over tetrahedrally coordinated cations. [b]For H_2O_t <2 wt%;

943 for H_2O_t >2 wt% ε3500 = 80 (±1) – 1.36 (±0.23) $C_{H_2O_t}$, where $C_{H_2O_t}$ is H_2O_t concentration in wt% (Leschik et al. 2004).

944 **Table 3: Rhyolite and Fe-bearing andesite hydrous glass standards.**

Oxide wt%	NWC	KRA-045-2	Run 10
SiO_2	76.45	72.17(22)	57.18(66)
TiO_2	0.06	0.53(02)	1.08(04)
Al_2O_3	12.32	14.07(08)	16.24(34)
FeO[a]	1.02	2.62(07)	4.75(33)
MnO	0.06	0.13(05)	0.00(-)
MgO	0.01	0.57(03)	3.28(07)
CaO	0.52	1.79(06)	7.39(13)
Na_2O	3.80	5.27(28)	3.01(09)
K_2O	4.75	2.46(13)	1.27(05)
P_2O_5	0.00	0.00(-)	0.00(-)
H_2O_t (manometry)	0.297	0.48	5.78
Total	99.29	100.09	99.98
Density (g/L)	2340	2395	2510
Wafer thickness (μm)	150 - 170	151	21

945

946 Notes: NWC composition from M. Humphreys (pers. comm.), manometry from Hauri
947 et al (2002), density from Newman et al (1986); KRA-045-2 composition from M.
948 Humphreys (pers. comm.), manometry and density from Maria and Luhr (2008); Run
949 10 composition, manometry and density from Mandeville et al (2002). Wafer thickness
950 measured at each FTIR analysis location by micrometer for NWC and KRA-045-2, and
951 by interference fringes in reflectance FTIR spectra for Run 10. Standard deviations
952 where known are given in parentheses in terms of least units reported e.g. 72.17(22)
953 indicates a standard deviation of 0.22 wt%. [a]Total Fe as FeO.

This is a preprint, the final version is subject to change, of the American Mineralogist (MSA)
Cite as Authors (Year) Title. American Mineralogist, in press.
(DOI will not work until issue is live.) DOI: http://dx.doi.org/10.2138/am-2017-5952CCBY

954 **Table 4: H_2O absorbance and concentration data from analyses of hydrous glass standards**

		Normalized absorbance (1/cm)			From 1630	Using species-dependent ε3500 method			From 4500	Manometry
Sample	**n**	**4500 cm^{-1} OH**	**3500 cm^{-1} H_2O_t**	**1630 cm^{-1} H_2O_m**	**H_2O_m (wt%)**	**OH (wt%)**	**H_2O_t (wt%)**	**ε3500 value**	**OH (wt%)**	**H_2O_t (wt%)**
NWC	12	0.552(110)	38.338(2.219)	2.674(443)	0.04(01)	0.27(02)	0.31(02)	94.7(9)	0.25(05)	0.297
KRA-045-2	12	0.790(073)	57.395(1.331)	5.326(898)	0.07(01)	0.39(01)	0.46(01)	93.1(1.1)	0.40(04)	0.48
Run 10	12	-	495.040(3.606)	216.270(5.116)	3.67(09)	2.23(03)	5.89(06)	60.3(3)	2.04(19)	5.78

955

956 Notes: Table shows the average normalized absorbance measured by FTIR in this study for each standard glass (n = number of analyses).
957 H_2O_m concentration from the 1630 cm^{-1} band and OH concentration from the 4500 cm^{-1} band are calculated in the conventional manner
958 via the Beer-Lambert law (Eq. 1, see Methods section for details). H_2O_m concentration from the 1630 cm^{-1} band is used in the species-
959 dependent ε3500 method (Eq. 4) to calculate the OH and H_2O_t concentrations and 'true' ε3500 value of each glass. H_2O_t concentrations
960 determined for each glass by manometry are shown for comparison (see Table 3 for details). Standard deviations are given in
961 parentheses in terms of least units reported.

This is a preprint, the final version is subject to change, of the American Mineralogist (MSA)
Cite as Authors (Year) Title. American Mineralogist, in press.
(DOI will not work until issue is live.) DOI: http://dx.doi.org/10.2138/am-2017-5952CCBY

Figure 1

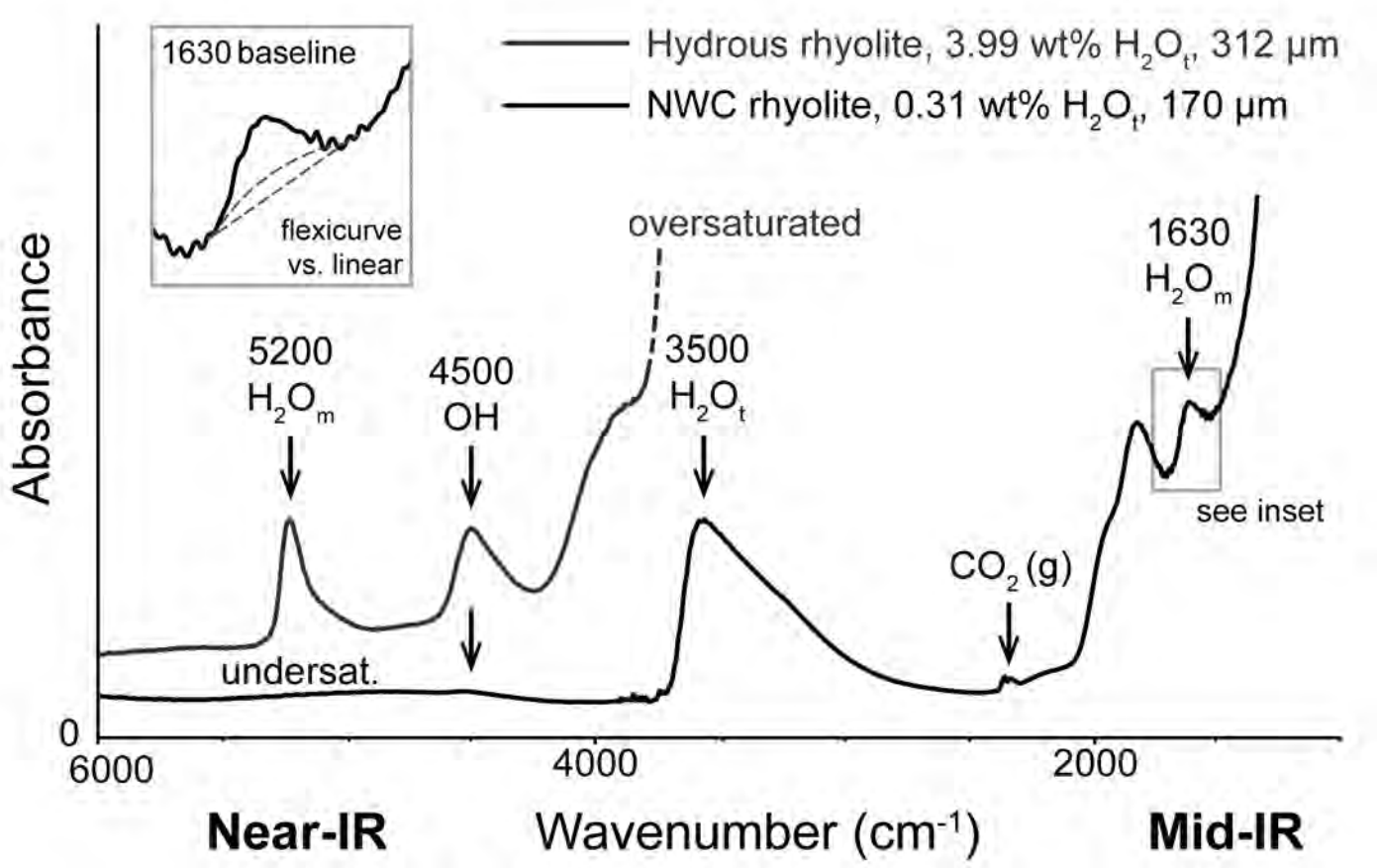

This is a preprint, the final version is subject to change, of the American Mineralogist (MSA)
Cite as Authors (Year) Title. American Mineralogist, in press.
(DOI will not work until issue is live.) DOI: http://dx.doi.org/10.2138/am-2017-5952CCBY

Figure 2

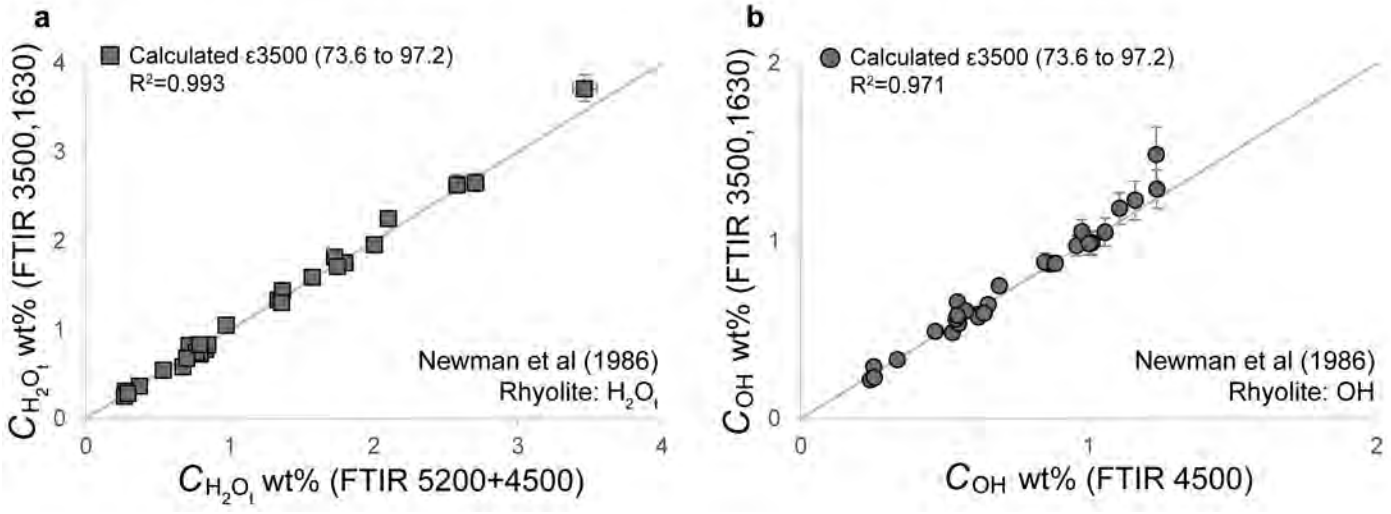

This is a preprint, the final version is subject to change, of the American Mineralogist (MSA)
Cite as Authors (Year) Title. American Mineralogist, in press.
(DOI will not work until issue is live.) DOI: http://dx.doi.org/10.2138/am-2017-5952CCBY

Figure 3

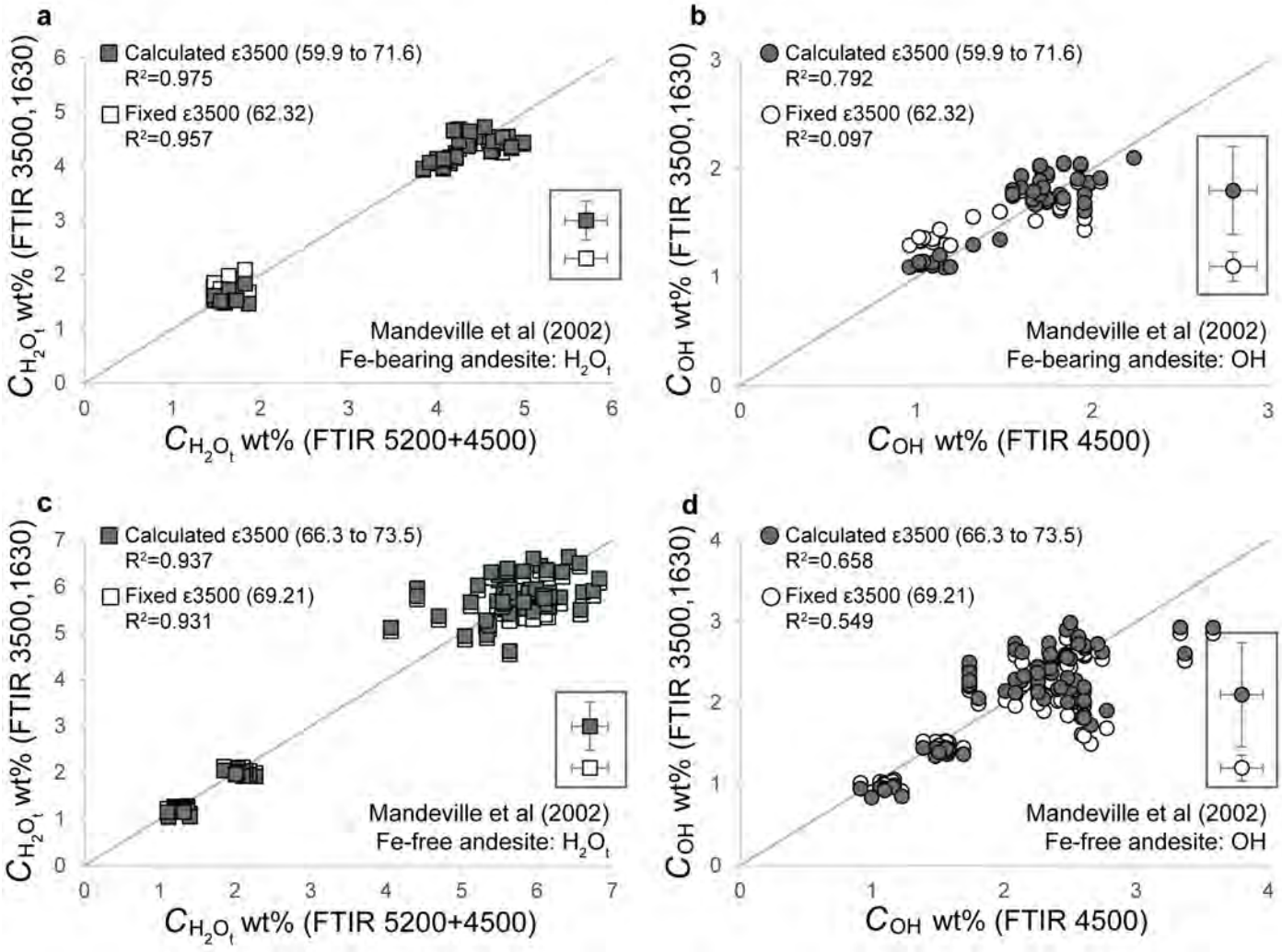

This is a preprint, the final version is subject to change, of the American Mineralogist (MSA)
Cite as Authors (Year) Title. American Mineralogist, in press.
(DOI will not work until issue is live.) DOI: http://dx.doi.org/10.2138/am-2017-5952CCBY

Figure 4

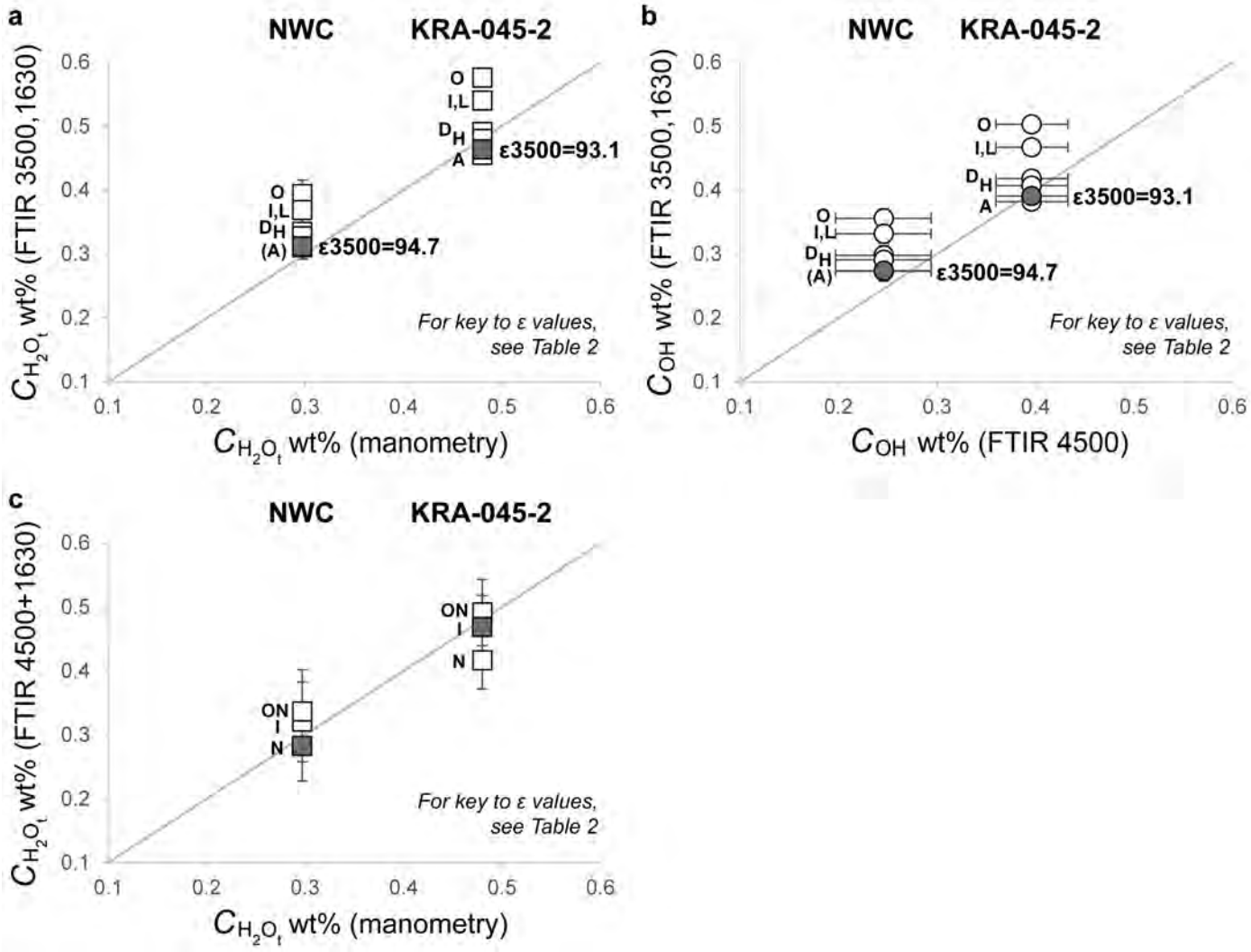

This is a preprint, the final version is subject to change, of the American Mineralogist (MSA)
Cite as Authors (Year) Title. American Mineralogist, in press.
(DOI will not work until issue is live.) DOI: http://dx.doi.org/10.2138/am-2017-5952CCBY

Figure 5

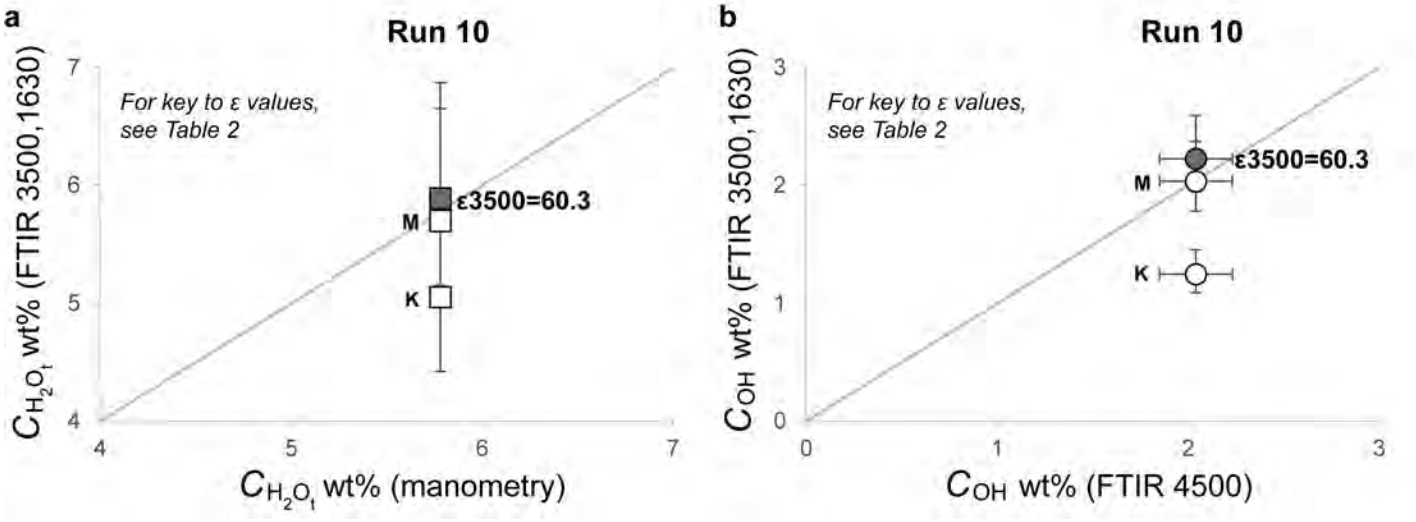

This is a preprint, the final version is subject to change, of the American Mineralogist (MSA)
Cite as Authors (Year) Title. American Mineralogist, in press.
(DOI will not work until issue is live.) DOI: http://dx.doi.org/10.2138/am-2017-5952CCBY

Figure 6

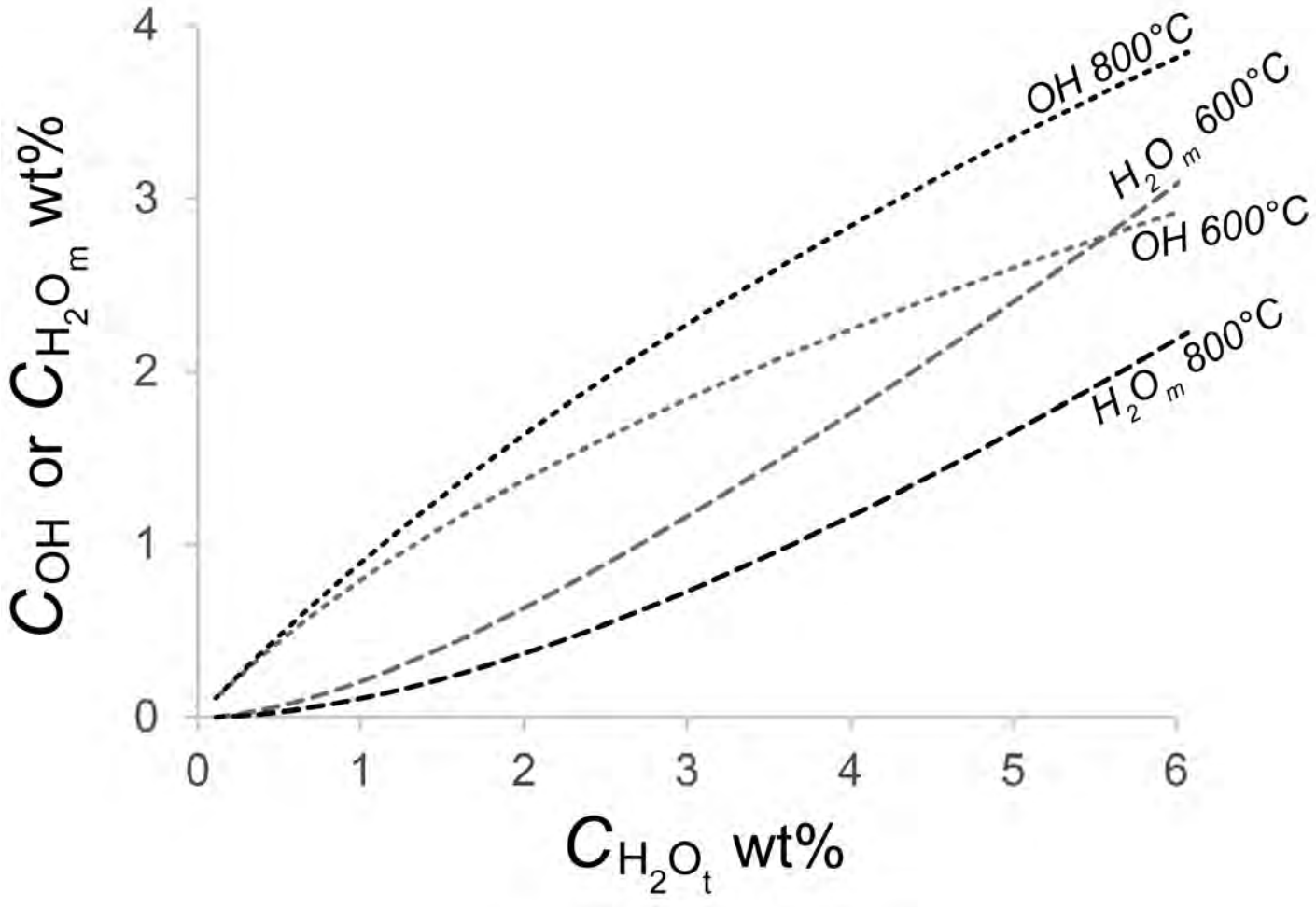

This is a preprint, the final version is subject to change, of the American Mineralogist (MSA)
Cite as Authors (Year) Title. American Mineralogist, in press.
(DOI will not work until issue is live.) DOI: http://dx.doi.org/10.2138/am-2017-5952CCBY

Figure 7